Cops-on-the-Dots: The Linear Stability of Crime Hotspots for a 1-D Reaction-Diffusion Model of Urban Crime

Andreas Buttenschoen* , Theodore Kolokolnikov† , Michael J. Ward‡ , Juncheng Wei§

September 14, 2018

Abstract

In a singularly perturbed limit, we analyze the existence and linear stability of steady-state hotspot solutions for an extension of the 1-D three-component reaction-diffusion (RD) system formulated and studied numerically in Jones et. al. [Math. Models. Meth. Appl. Sci., **20**, Suppl., (2010)], which models urban crime with police intervention. In our extended RD model, the field variables are the attractiveness field for burglary, the criminal density, and the police density, and it includes a scalar parameter that determines the strength of the police drift towards maxima of the attractiveness field. For a special choice of this parameter, we recover the "cops-on-the-dots" policing strategy of Jones et. al., where the police mimic the drift of the criminals towards maxima of the attractiveness field. For our extended model, the method of matched asymptotic expansions is used to construct 1-D steady-state hotspot patterns as well as to derive nonlocal eigenvalue problems (NLEPs), each having three distinct nonlocal terms, that characterize the linear stability of these hotspot steady-states to $\mathcal{O}(1)$ time-scale instabilities. For a cops-on-the-dots policing strategy, where some key identities can be used to recast these NLEPs into equivalent NLEPs with only one nonlocal term, we prove that a multi-hotspot steady-state is linearly stable to synchronous perturbations of the hotspot amplitudes. Moreover, for asynchronous perturbations of the hotspot amplitudes, a hybrid analytical-numerical method is used to construct linear stability phase diagrams in the police versus criminal diffusivity parameter space. In one particular region of these phase diagrams, the hotspot steady-states are shown to be unstable to asynchronous oscillatory instabilities in the hotspot amplitudes that arise from a Hopf bifurcation. Within the context of our model, this provides a parameter range where the effect of a cops-on-the-dots policing strategy is to only displace crime temporally between neighboring spatial regions. Our hybrid approach to study the equivalent NLEP combines rigorous spectral results with a numerical parameterization of any Hopf bifurcation threshold. For the cops-on-the-dots policing strategy, our linear stability predictions for steady-state hotspot patterns are confirmed from full numerical PDE simulations of the three-component RD system.

Key Words: Urban crime, hotspot patterns, nonlocal eigenvalue problem (NLEP), Hopf bifurcation, asynchronous oscillatory instability, cops-on-the-dots.

1   Introduction

Motivated by the increased availability of residential burglary data, the development of mathematical modeling approaches to quantify and predict spatial patterns of urban crime was initiated in [18–20]. One primary feature incorporated into these models, which is based on observations from the available data (cf. [4]), is that spatial patterns of residential burglary are typically concentrated in small regions known as hotspots; a feature believed to be attributable to a repeat or near-repeat victimization effect (cf. [9], [29]). There have been two primary frameworks that have been used to model the effect of police intervention on crime hotspot patterns. One approach, ideal for incorporating detailed real-world policing strategies, is large scale simulations of agent-based models (cf. [10], [5]). However, with this approach, it is difficult to isolate the effect of

---

*Dept. of Mathematics, UBC, Vancouver, Canada. `abuttens@math.ubc.ca`
†Dept. of Mathematics and Statistics, Dalhousie, Halifax, Canada. `tkolokol@gmail.com`
‡Dept. of Mathematics, UBC, Vancouver, Canada. (corresponding author `ward@math.ubc.ca`)
§Dept. of Mathematics, UBC, Vancouver, Canada. `jcwei@math.ubc.ca`

changes in the model parameters. A second, more phemenological approach, is to formulate PDE-based reaction-diffusion (RD) systems that model the police density as an extra field variable (cf. [10], [15], [16]). More elaborate PDE models, such as in [30], formulate an optimal control strategy to minimize the overall crime rate by allowing the police to adapt to dynamically evolving crime patterns.

In our PDE-based approach, motivated by [10] and [16], the police intervention is modeled by a drift-diffusion PDE, in which a parameter models the strength of the drift towards the maxima of the attractiveness field for burglary. For this three-component RD system consisting of an attractiveness field coupled to the criminal and police densities, we will study the existence and linear stability properties of steady-state hotspot patterns on a 1-D spatial domain $0 < x < S$ in a singularly perturbed limit. The specific three-component RD model of urban crime that we will analyze is formulated as

$$A_t = \epsilon^2 A_{xx} - A + \rho A + \alpha \,, \tag{1.1a}$$

$$\rho_t = D \left(\rho_x - 2\rho A_x/A\right)_x - \rho A + \gamma - \alpha - \rho U \,, \tag{1.1b}$$

$$\tau U_t = D \left(U_x - q U A_x/A\right)_x \,, \tag{1.1c}$$

where $A_x = \rho_x = U_x = 0$ at $x = 0, S$. Here A is the attractiveness field for burglary, while ρ and U are the densities of criminals and police, respectively. In this model, α is the baseline attractiveness, $\gamma - \alpha > 0$ is the rate at which new criminals are introduced, D is the criminal diffusivity, $D_p \equiv D/\tau$ is the police diffusivity, and $\epsilon \ll 1$ characterizes the repeat or near-repeat victimization effect (cf. [18], [9], [29]). For (1.1c), the total policing level U_0 is prescribed, and it satisfies

$$U_0 \equiv \int_0^S U(x,t) \, dx \,, \tag{1.2}$$

so that it is conserved in time. The model parameters α, $\gamma - \alpha$, D, D_p, and U_0 are all assumed to be positive constants.

In (1.1), the parameter $q > 0$ measures the degree of focus in the police patrol towards maxima of the attractiveness field. The choice $q = 2$, which recovers the PDE system derived and studied numerically in [10], is the "cops-on-the-dots" strategy (cf. [10], [16]) where the police mimic the drift of the criminals towards maxima of A. In (1.1b), the police density at a given spatial location decreases the local criminal population at a rate proportional to the local criminal density (the $-\rho U$ term in (1.1b)). The resulting predator-prey type police interaction model (1.1) is to be contrasted with the "simple police interaction" model formulated in [16], and analyzed in [22], where the $-\rho U$ term in (1.1b) is replaced by $-U$.

In the absence of police, i.e. $U_0 = 0$, (1.1) reduces to the two-component PDE system for A and ρ first derived and studied in [18] and [20]. Pattern formation aspects for this "basic" crime model have been well-studied from various viewpoints, including, weakly nonlinear theory (cf. [19]), bifurcation theory near Turing points (cf. [6], [8]) and the computation of global snaking-type bifurcation diagrams (cf. [13]), rigorous existence theory (cf. [17]), and asymptotic methods for constructing steady-state hotspot patterns whose linear stability properties can be analyzed via NLEP theory (cf. [11], [1], [21]).

Our goal here is to extend the analysis given in [22] for the existence and linear stability of hotspot steady-states for the simple police interaction model to the predator-prey type interaction model (1.1). We will show that the seemingly minor and innocuous replacement of $-U$ from the model in [22] with $-\rho U$ in (1.1b) leads to a significantly more challenging linear stability problem for hotspot equilibria. This is discussed in detail below.

As in [22] and [11], we will analyze (1.1) in the limit $\epsilon \to 0$ for the range $D = \mathcal{O}(\epsilon^{-2})$. Since $A = \mathcal{O}(\epsilon^{-1})$ in the core of the hotspot, it convenient as in [22] to introduce the new variables v and u by

$$\rho = \epsilon^2 v A^2 \,, \qquad U = u A^q \,, \qquad D = \epsilon^{-2} \mathcal{D} \,. \tag{1.3}$$

In terms of A, v, and u, on the domain $0 < x < S$, and with no flux boundary conditions at $x = 0, S$, (1.1) transforms to

$$A_t = \epsilon^2 A_{xx} - A + \epsilon^2 v A^3 + \alpha \,, \tag{1.4a}$$

$$\epsilon^2 \left(A^2 v \right)_t = \mathcal{D} \left(A^2 v_x \right)_x - \epsilon^2 v A^3 + \gamma - \alpha - \epsilon^2 uv A^{2+q} \,, \tag{1.4b}$$

$$\tau \epsilon^2 \left(A^q u \right)_t = \mathcal{D} \left(A^q u_x \right)_x \,, \tag{1.4c}$$

where the police diffusivity D_p becomes $D_p = \epsilon^{-2} \mathcal{D}/\tau$.

In §2 we use a formal singular perturbation analysis in the limit $\epsilon \to 0$ to construct hotspot steady-state solutions to (1.4) that have a common amplitude. Our steady-state analysis is restricted to the range $q > 1$, for which the police density is asymptotically small in the background region away from the hotspots. In Proposition 2.1 and Corollary 2.2 below we establish that steady-state hotspot solutions exist only when $U_0 < U_{0,\max} \equiv S(\gamma - \alpha)(q + 1)/(2q)$.

In §3 we use a singular perturbation analysis combined with Floquet theory, similar to but more intricate than that used in [22] and [11], to derive two distinct NLEP spectral problems characterizing the linear stability of hotspot steady-states of (1.4). One such NLEP, given below in Proposition 3.2, characterizes the linear stability properties of a multi-hotspot steady state solution, having $K \geq 2$ hotspots, to synchronous perturbations in the hotspot amplitudes. The linear stability properties of a one-hotspot steady-state is also determined by the spectrum of this NLEP. In addition, the second NLEP, given below in Proposition 3.4, characterizes the linear stability properties of a multi-hotspot steady-state, with $K \geq 2$ hotspots, to $K - 1 > 0$ different spatial modes of asynchronous perturbations of the hotspot amplitudes. A complicating feature in the analysis of these spectral problems is that each of the two NLEPs has *three distinct nonlocal* terms consisting of a linear combination of $\int w^2 \Phi$, $\int w^{q-1} \Phi$, and $\int w^{q+1} \Phi$. Here $w(y) = \sqrt{2} \operatorname{sech} y$ is the homoclinic profile of a hotspot, and $\Phi(y)$ is the NLEP eigenfunction. As a result of this complexity, the determination of unstable spectra for these NLEPs is seemingly beyond the general NLEP stability theory with a single nonlocal term, as surveyed in [28]. For the simple police interaction model, studied in [22], the corresponding NLEPs had only two nonlocal terms.

In §4 we use a hybrid analytical-numerical strategy to determine the spectrum of the NLEP characterizing the linear stability to synchronous perturbations. For arbitrary $q > 1$, the two different approaches developed in §4.1 and §4.2 provide clear numerical evidence that this NLEP has no unstable eigenvalues. This strongly indicates that, for any $q > 1$, a one-hotspot steady-state is always linearly stable and that a multi-hotspot steady-state is always linearly stable to synchronous perturbations in the hotspot amplitudes. For the special case $q = 2$ of "cops-on-the-dots", in §4.2.1 this linear stability conjecture is proved rigorously. This proof of linear stability for $q = 2$ relies on some key identities that allow the NLEP with three nonlocal terms to be converted into an equivalent NLEP with a single nonlocal term.

For general $q > 1$, in §5 we determine the threshold value of $\mathcal{D}$ corresponding to a zero-eigenvalue crossing of the NLEP, as defined in Proposition 3.4, that characterizes the linear stability of a multi-hotspot steady-state to the asynchronous modes. For a K-hotspot steady-state with $K \geq 2$, this critical value of $\mathcal{D}$, called the competition stability threshold, is

$$\mathcal{D}_c \equiv \frac{S}{8K^4 \pi^2 \alpha^2 \left[1 + \cos \left(\pi/K \right) \right]} \left[(1 - q)\omega^3 + qS(\gamma - \alpha)\omega^2 \right] \,, \qquad \text{where} \quad \omega \equiv S(\gamma - \alpha) - 2qU_0/(q + 1) \,, \tag{1.5}$$

on $U_0 < U_{0,\max} \equiv S(\gamma - \alpha)(q + 1)/(2q)$. In the limiting case of an infinite police diffusivity, a winding number analysis is used in §5.1 to prove, for an arbitrary $q > 1$, that a multi-hotspot steady-state is linearly stable to asynchronous perturbations in the hotspot amplitudes if and only if $\mathcal{D} < \mathcal{D}_c$ (see Proposition 5.2 below).

For the special case $q = 2$ of "cops-on-the-dots", in §6 we show how to transform the NLEP for the asynchronous modes into an equivalent NLEP with only one nonlocal term, which is then more readily analyzed. With this reduction of the NLEP into a more standard form, which only applies when $q = 2$, in Proposition 6.4 we prove that a K-hotspot

3

steady-state, with $K \geq 2$, is always unstable to the asynchronous modes when $\mathcal{D} > \mathcal{D}_c$ for any police diffusivity $D_p > 0$. Moreover, from a numerical parameterization of branches of purely complex eigenvalues for this equivalent NLEP, we show that each of the $K-1$ asynchronous modes can undergo a Hopf bifurcation at some critical values of the police diffusivity D_p defined on some intervals of $\mathcal{D}$. Overall, this hybrid approach provides phase diagrams in the ϵD_p versus $\mathcal{D}$ parameter plane characterizing the linear stability of the hotspot steady-states to asynchronous perturbations in the hotspot amplitudes. Numerical evidence from PDE simulations suggests that hotspot amplitude oscillations arising from the Hopf bifurcation can be either subcritical or supercritical, depending on the parameter set. Linear stability phase diagrams for various U_0 are shown below in Fig. 9 and Fig. 10 for $K = 2$ and $K = 3$, respectively. One key qualitative feature derived from these phase diagrams is that there is a region in the ϵD_p versus $\mathcal{D}$ parameter space where the effect of police intervention is to only displace crime temporally between neighboring spatial regions; a phenomenon qualitatively consistent with the field observations reported in [3] for a "cops-on-the-dots" policing strategy.

As in [22], we emphasize that the interval in $\mathcal{D}$ where asynchronous hotspot amplitude oscillations occur disappears when $U_0 = 0$. Therefore, it is the third component of the RD system (1.4) that is needed to support these temporal oscillations. In contrast, for most two-component RD systems with localized spike-type solutions, such as the the Gray-Scott and Gierer-Meinhardt models (cf. [7], [14], [23], [12]), the dominant Hopf stability threshold for spike amplitude oscillations, based on an NLEP linear stability analysis, is determined by the spatial mode that synchronizes the oscillations.

For $q = 2$, in §7 we validate the predictions of our linear stability analysis with full numerical PDE simulations of (1.4). Finally, in §8 we compare our linear stability results for (1.4) for a "cops-on-the-dots" strategy with those in [22] for the simple police interaction model. We also briefly discuss some specific open problems and new directions warranting study.

2 Asymptotic Construction of a Multiple Hotspot Steady-State

In the limit $\epsilon \to 0$, we use the method of matched asymptotic expansions to construct a steady-state solution to (1.4) on $0 \leq x \leq S$ with $K \geq 1$ interior hotspots of a common amplitude. We follow the approach in [22] in which we first construct a one-hotspot solution to (1.4) centered at $x = 0$ on the reference domain $|x| \leq l$. From translation invariance, this construction yields a K interior hotspot steady-state solution on the original domain of length $S = (2\ell)K$. On $|x| \leq \ell$, (1.2) yields that $\int_{-\ell}^{\ell} U \, dx = U_0/K$, where U_0 is the constant total police deployment.

On the reference domain $|x| \leq l$, we center a steady-state hotspot at $x = 0$, and we impose $A_x = v_x = u_x = 0$ at $x = \pm l$. For this *canonical* hotspot problem, the steady-state problem for (1.4) is to find $A(x)$, $v(x)$, and the constant u, satisfying

$$\epsilon^2 A_{xx} - A + \epsilon^2 v A^3 + \alpha = 0, \qquad |x| \leq \ell; \qquad A_x = 0, \quad x = \pm \ell, \tag{2.1a}$$

$$\mathcal{D} \left(A^2 v_x \right)_x - \epsilon^2 v A^3 + \gamma - \alpha - \epsilon^2 u v A^{2+q} = 0, \qquad |x| \leq \ell; \qquad v_x = 0, \quad x = \pm \ell, \tag{2.1b}$$

where the steady-state police density $U(x)$ is related to u by

$$U = u A^q, \qquad \text{where} \qquad u = \frac{U_0}{K \int_{-\ell}^{\ell} A^q \, dx}. \tag{2.2}$$

For $\epsilon \to 0$, we have $A \sim \alpha + \mathcal{O}(\epsilon^2)$ in the outer region, while in the inner region near $x = 0$, we set $y = \epsilon^{-1}x$ and expand $A \sim \epsilon^{-1}A_0$ and $v \sim v_0$ in (2.1). To leading-order, in the inner region we obtain from (2.1) that

$$A_0 \sim \frac{w(y)}{\sqrt{v_0}}, \qquad v \sim v_0. \tag{2.3}$$

Here v_0 is a constant to be determined and $w(y) = \sqrt{2}\,\text{sech}\,y$ is the homoclinic solution of

$$w'' - w + w^3 = 0\,, \qquad -\infty < y < \infty\,; \qquad w(0) > 0\,, \quad w'(0) = 0\,, \quad w \to 0 \quad \text{as} \quad y \to \pm\infty\,. \tag{2.4}$$

Integrals of various powers of $w(y)$, as needed below, can be calculated in terms of the Gamma function $\Gamma(z)$ by (cf. [22])

$$I_q \equiv \int_{-\infty}^{\infty} w^q \, dy = 2^{3q/2-1} \frac{[\Gamma(q/2)]^2}{\Gamma(q)}\,. \tag{2.5}$$

We will consider the range $q > 1$ where the dominant contribution to the integral $\int_{-\ell}^{\ell} A^q \, dx$ arises from the inner region:

$$\int_{-\ell}^{\ell} A^q \, dx \sim \epsilon^{1-q} v_0^{-q/2} \int_{-\infty}^{\infty} w^q \, dy = \mathcal{O}(\epsilon^{1-q}) \gg 1\,.$$

Since $q > 1$, (2.2) shows that u depends to leading-order only on the inner region contribution from A^q. For $\epsilon \ll 1$, we get

$$u \sim \epsilon^{q-1} \tilde{u}_e\,, \qquad \text{where} \qquad \tilde{u}_e \equiv \frac{U_0 v_0^{q/2}}{K I_q}\,. \tag{2.6}$$

To determine v_0, we integrate (2.1b) over $-\ell < x < \ell$, while imposing $v_x(\pm\ell) = 0$. This yields that

$$\epsilon^2 \int_{-\ell}^{\ell} v A^3 \, dx = 2\ell\,(\gamma - \alpha) - \epsilon^2 u \int_{-\ell}^{\ell} v A^{2+q} \, dx\,. \tag{2.7}$$

Since $A \sim \alpha = \mathcal{O}(1)$ and $A = \mathcal{O}(\epsilon^{-1})$ in the outer and inner regions, respectively, it follows that, when $q > 1$, the dominant contribution to the integral arises from the inner region where $v \sim v_0$. In this way, and by using (2.2) in (2.7), we get

$$\frac{\int_{-\infty}^{\infty} w^3 \, dy}{\sqrt{v_0}} \sim 2\ell\,(\gamma - \alpha) - \frac{\epsilon^2 U_0 v_0}{K} \frac{\int_{-\ell}^{\ell} A^{2+q} \, dx}{\int_{-\ell}^{\ell} A^q \, dx}\,. \tag{2.8}$$

By using $A \sim \epsilon^{-1} w(y)/\sqrt{v_0}$, together with (2.5), we calculate the integral ratio in (2.8) for $\epsilon \to 0$ as

$$\frac{\int_{-\ell}^{\ell} A^{2+q} \, dx}{\int_{-\ell}^{\ell} A^q \, dx} \sim \frac{\epsilon^{-2}}{v_0} \frac{\int_{-\infty}^{\infty} w^{q+2} \, dy}{\int_{-\infty}^{\infty} w^q \, dy} = \frac{\epsilon^{-2}}{v_0} \frac{2^{3(q+2)/2-1}}{2^{3q/2-1}} \left(\frac{\Gamma(1+q/2)}{\Gamma(q/2)}\right)^2 \frac{\Gamma(q)}{\Gamma(q+2)} = \frac{\epsilon^{-2}}{v_0} \frac{2q}{q+1}\,, \tag{2.9}$$

by using $\Gamma(x+1) = x\Gamma(x)$. Then, by substituting (2.9) into (2.8), and using $\int_{-\infty}^{\infty} w^3 \, dy = \sqrt{2}\pi$, we solve for v_0 to get

$$v_0 = 2\pi^2 \left[2\ell(\gamma - \alpha) - \frac{U_0}{K} \frac{2q}{q+1}\right]^{-2}\,, \tag{2.10}$$

provided that the total level U_0 of police deployment is below a threshold given by

$$U_0 < U_{0,max} \equiv 2\ell K\,(\gamma - \alpha)\,\frac{(q+1)}{2q} = S(\gamma - \alpha)\frac{(q+1)}{2q}\,. \tag{2.11}$$

Here $S = 2\ell K$ is the original domain length. We will assume that (2.11) holds, so that a K-hotspot steady-state exists. The amplitude of the hotspot, defined by $A_{\max} \equiv A(0) \gg 1$, is given by

$$A_{\max} \equiv A(0) \sim \epsilon^{-1} A_0(0) = \epsilon^{-1} \frac{w(0)}{\sqrt{v_0}} = \frac{\epsilon^{-1}\omega}{\pi K}\,, \qquad \text{where} \qquad \omega \equiv S(\gamma - \alpha) - U_0 \frac{2q}{q+1}\,. \tag{2.12}$$

This hotspot amplitude decreases with increasing either K, U_0, or q.

To complete the asymptotic construction of the hotspot, in the outer region we expand $v \sim v_e(x) + \ldots$ and use $A \sim \alpha + \mathcal{O}(\epsilon^2)$. From (2.1b), we obtain to leading order that $v_e(x)$ satisfies

$$\mathcal{D}v_{exx} = -\frac{(\gamma - \alpha)}{\alpha^2}\,, \qquad -\ell < x < \ell\,; \qquad v_e(0) = v_0\,, \qquad v_{ex}(\pm\ell) = 0\,, \tag{2.13}$$

which is readily solved analytically. We summarize our leading-order results for a steady-state K-hotspot pattern as follows:

Proposition 2.1 *Let $\epsilon \to 0$, $q > 1$, and $0 < U_0 < U_{0,\max}$, where $U_{0,\max}$ is given in (2.11). Then, (1.4) admits a steady-state solution on $(0, S)$ with K interior hotspots of a common amplitude. On each sub-domain of length $2\ell = S/K$, and translated to $(-\ell, \ell)$ to contain exactly one hotspot at $x = 0$, the steady-state solution, to leading order, is given by*

$$A \sim \frac{w(x/\epsilon)}{\epsilon\sqrt{v_0}}, \quad \text{if} \quad x = \mathcal{O}(\epsilon); \qquad A \sim \alpha, \quad \text{if} \quad x = \mathcal{O}(1), \tag{2.14a}$$

$$v \sim v_e = \frac{\zeta}{2}\left[(\ell - |x|)^2 - \ell^2\right] + v_0, \qquad \text{where} \quad v_0 = 2\pi^2 K^2\left[S(\gamma - \alpha) - U_0\frac{2q}{q+1}\right]^{-2}, \tag{2.14b}$$

$$u \sim \epsilon^{q-1}\tilde{u}_e, \qquad \text{where} \quad \tilde{u}_e \equiv \frac{U_0 v_0^{q/2}}{K I_q} \quad \text{and} \quad I_q \equiv \int_{-\infty}^{\infty} w^q \, dy = 2^{3q/2 - 1}\frac{[\Gamma(q/2)]^2}{\Gamma(q)}. \tag{2.14c}$$

Here $w(y) = \sqrt{2}\,\mathrm{sech}\,y$ is the homoclinic of (2.4) and $\zeta \equiv -(\gamma - \alpha)/(\mathcal{D}\alpha^2)$.

In terms of the criminal and police densities, given by $\rho = \epsilon^2 v A^2$ and $U = uA^q$ from (1.3), we have the following:

Corollary 2.2 *Under the same conditions as in Proposition 2.1, (2.14) yields to leading-order that*

$$A \sim \frac{w(x/\epsilon)}{\epsilon\sqrt{v_0}}, \quad \text{if} \quad x = \mathcal{O}(\epsilon); \qquad A \sim \alpha, \quad \text{if} \quad \mathcal{O}(\epsilon) \ll |x| < \ell, \tag{2.15a}$$

$$\rho \sim [w(x/\epsilon)]^2, \quad \text{if} \quad x = \mathcal{O}(\epsilon); \qquad \rho \sim \epsilon^2 v_e \alpha^2, \quad \text{if} \quad \mathcal{O}(\epsilon) \ll |x| < \ell, \tag{2.15b}$$

$$U \sim \frac{U_0}{\epsilon K I_q}[w(x/\epsilon)]^q, \quad \text{if} \quad x = \mathcal{O}(\epsilon); \qquad U \sim \epsilon^{q-1}\alpha^q\frac{U_0 v_0^{q/2}}{K I_q}, \quad \text{if} \quad \mathcal{O}(\epsilon) \ll |x| < \ell, \tag{2.15c}$$

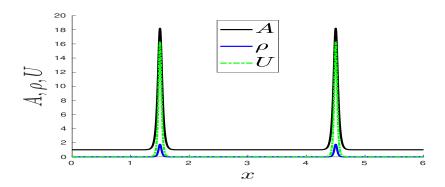*where v_e and v_0 are given in (2.14) and $w(y) = \sqrt{2}\,\mathrm{sech}\,y$.*

Figure 1:   The steady-state two-hotspot solution for $S = 6$, $\gamma = 2$, $\alpha = 1$, $U_0 = 2$, $\epsilon = 0.03$, $\mathcal{D} = 0.3$, $D_p \approx 16.667$, for the "cops-on-the-dots" $q = 2$ patrol. Plot is the steady-state solution corresponding to the left panel of Fig. 11 below.

In Fig. 1 we use (2.15) to plot a two-hotspot steady-state solution for a particular parameter set. This plot clearly shows the concentration behavior of A, ρ, and U near the hotspot locations.

From (2.15), we observe that the criminal density near a hotspot is independent of the total police deployment U_0 and patrol focus q. Since $q > 1$, the police density $U(x)$ is small in the outer region, but is asymptotically large near a hotspot.

We observe that our leading-order asymptotic result in (2.15) for the hotspot steady-state is equivalent to simply replacing U_0 in Proposition 2.1 and Corollary 2.2 of [22] with $2qU_0/(q+1)$. Since $2q/(q+1) > 1$ for $q > 1$, we conclude that, for the same parameter values and level U_0 of total police deployment, the steady-state hotspot amplitude is smaller for the RD model (1.4) with predator-prey type police interaction than for the RD model of [22] with simple police interaction.

6

3   The NLEP for a K-Hotspot Steady-State Pattern

To analyze the linear stability of a K-hotspot steady-state solution, we must extend the singular perturbation approach used in [22] to derive the corresponding nonlocal eigenvalue problem (NLEP). This is done by first deriving the NLEP for a one-hotspot solution on the reference domain $|x| \leq \ell$, subject to Floquet-type boundary conditions imposed at $x = \pm \ell$. In terms of this canonical problem, the NLEP for the finite-domain problem $0 < x < S$ with Neumann conditions at $x = 0, S$ is then readily recovered as in [22] (see also [11]). Since the analysis to derive the NLEP is similar to that in [22], we only outline it below. Further details on the derivation of the NLEP are given in Appendix A.

3.1   Linearization with Floquet Boundary Conditions

Let (A_e, v_e, u_e) denote the steady-state with a single hotspot centered at $x = 0$ in $|x| \leq \ell$. We introduce the perturbation

$$A = A_e + e^{\lambda t}\phi, \qquad v = v_e + e^{\lambda t}\epsilon\psi, \qquad u = u_e + e^{\lambda t}\epsilon^q\eta, \tag{3.1}$$

where the asymptotic orders of the perturbations ($\mathcal{O}(1)$, $\mathcal{O}(\epsilon)$ and $\mathcal{O}(\epsilon^q)$) are chosen so that ϕ, ψ, and η are all $\mathcal{O}(1)$ in the inner region. By substituting (3.1) into (1.4) and linearizing, we obtain that

$$\epsilon^2\phi_{xx} - \phi + 3\epsilon^2 v_e A_e^2\phi + \epsilon^3 A_e^3\psi = \lambda\phi, \tag{3.2a}$$

$$\mathcal{D}\left(2A_e v_{ex}\phi + \epsilon A_e^2\psi_x\right)_x - 3\epsilon^2 A_e^2 v_e\phi - \epsilon^3 A_e^3\psi - \epsilon^2(2+q)u_e v_e A_e^{q+1}\phi - \epsilon^{2+q}v_e A_e^{2+q}\eta - \epsilon^3 u_e A_e^{2+q}\psi$$
$$= \lambda\epsilon^2\left(2A_e v_e\phi + \epsilon A_e^2\psi\right), \tag{3.2b}$$

$$\mathcal{D}\left(qA_e^{q-1}u_{ex}\phi + \epsilon^q A_e^q\eta_x\right)_x = \epsilon^2\tau\lambda\left(qA_e^{q-1}u_e\phi + \epsilon^q A_e^q\eta\right). \tag{3.2c}$$

As in [22], for $K \geq 2$, we impose Floquet-type boundary conditions at $x = \pm\ell$ for the long-range components ψ and η

$$\begin{pmatrix} \eta(\ell) \\ \psi(\ell) \end{pmatrix} = z\begin{pmatrix} \eta(-\ell) \\ \psi(-\ell) \end{pmatrix}, \qquad \begin{pmatrix} \eta_x(\ell) \\ \psi_x(\ell) \end{pmatrix} = z\begin{pmatrix} \eta_x(-\ell) \\ \psi_x(-\ell) \end{pmatrix}. \tag{3.3}$$

Here z is a complex-valued parameter. We will consider the case of a single hotspot, where $K = 1$, separately in §3.2 below.

For $K \geq 2$, the NLEP associated with a K-hotspot pattern on $[-l, (2K-1)l]$ with *periodic boundary conditions*, on a domain of length $2Kl$, is obtained by setting $z^K = 1$, which yields $z_j = e^{2\pi ij/K}$ for $j = 0, \ldots, K-1$. For these values of z_j in (3.3) we obtain the spectral problem for the linear stability of a K-hotspot solution on a domain of length $2Kl$ with periodic boundary conditions. To relate the spectra of the periodic problem to the Neumann problem, in such a way that the Neumann problem is still posed on a domain of length S, we proceed as in §3 of [22] (see also §3 of [11]). There it was shown that we need only replace $2K$ with K in the definition of z_j. In this way, the Floquet parameters in (3.3) for a hotspot steady-state on a domain of length $S = 2lK$, having $K \geq 2$ interior hotspots and Neumann boundary conditions at $x = 0$ and $x = S$ is $z = z_j \equiv e^{\pi ij/K}$ for $j = 0, \ldots, K-1$. For these values of z, the following identity is needed below:

$$\frac{(z-1)^2}{2z} = \text{Re}(z) - 1 = \cos\left(\frac{\pi j}{K}\right) - 1, \qquad j = 0, \ldots, K-1. \tag{3.4}$$

We now begin our derivation of the NLEP. For (3.2a), in the inner region where $A_e \sim \epsilon^{-1}w/\sqrt{v_0}$, $v_e \sim v_0$, and $\psi \sim \psi(0) \equiv \psi_0$, it follows that the leading-order term $\Phi(y) = \phi(\epsilon y)$ in the inner expansion of ϕ satisfies

$$\Phi'' - \Phi + 3w^2\Phi + \frac{\psi(0)}{v_0^{3/2}}w^3 = \lambda\Phi. \tag{3.5}$$

In the outer region $\epsilon \ll |x| \le \ell$, to leading order we obtain from (3.2) that

$$\phi \sim \epsilon^3 \alpha^3 \psi / [\lambda + 1 - 3\epsilon^2 \alpha^2 v_e] = \mathcal{O}(\epsilon^3), \qquad \psi_{xx} \approx 0, \qquad \eta_{xx} \approx 0. \tag{3.6}$$

The goal of the calculation below is to determine $\psi(0)$, which from (3.5) yields the NLEP. To do so, we must derive appropriate jump conditions for ψ_x and η_x across the hotspot region centered at $x = 0$. This calculation, summarized in Appendix A, then leads to linear BVP problems for ψ and η, from which we can calculate $\psi(0)$.

As shown in Appendix A, we obtain that the outer approximation for $\psi(x)$ satisfies

$$\psi_{xx} = 0, \quad |x| \le \ell; \qquad e_0 [\psi_x]_0 = e_1 \psi(0) + e_2 \eta(0) + e_3, \quad \psi(\ell) = z\psi(-\ell), \quad \psi_x(\ell) = z\psi_x(-\ell), \tag{3.7a}$$

where we have defined $[a]_0 \equiv a(0^+) - a(0^-)$. Defining $\int (\dots) \equiv \int_{-\infty}^{\infty} (\dots) \, dy$, the coefficients e_j, for $j = 0, \dots, 3$, are

$$e_0 \equiv \mathcal{D}\alpha^2, \qquad e_1 \equiv \frac{1}{v_0^{3/2}} \int w^3 + \frac{\tilde{u}_e}{v_0^{1+q/2}} \int w^{q+2},$$

$$e_2 \equiv \frac{1}{v_0^{q/2}} \int w^{2+q}, \qquad e_3 \equiv 3 \int w^2 \Phi + \frac{\tilde{u}_e}{v_0^{(q-1)/2}} (q+2) \int w^{q+1} \Phi. \tag{3.7b}$$

This BVP (3.7) is defined in terms of $\eta(0)$, which must be found from a separate BVP (see Appendix A). To achieve a distinguished balance in this BVP we introduce $\hat{\tau} = \mathcal{O}(1)$ by $\hat{\tau} \equiv \epsilon^{3-q}\tau$, so that the police diffusivity $D_p \equiv \epsilon^{-2}\mathcal{D}/\tau$ becomes

$$D_p \equiv \epsilon^{1-q}\mathcal{D}/\hat{\tau}, \qquad \text{where} \qquad \hat{\tau} \equiv \epsilon^{3-q}\tau. \tag{3.8}$$

In terms of $\hat{\tau}$, we determine $\eta(0)$ from the following BVP, as derived in Appendix A:

$$\eta_{xx} = 0, \quad |x| \le \ell; \qquad d_0 [\eta_x]_0 = d_1 \eta(0) + d_2, \quad \eta(\ell) = z\eta(-\ell), \quad \eta_x(\ell) = z\eta_x(-\ell). \tag{3.9a}$$

In terms of v_0 and $\tilde{u}_e$, as defined in (2.14), the constants d_0, d_1, and d_2, are defined by

$$d_0 \equiv \mathcal{D}\alpha^q, \qquad d_1 \equiv \frac{\hat{\tau}\lambda}{v_0^{q/2}} \int w^q, \qquad d_2 \equiv \frac{\hat{\tau}\lambda q \tilde{u}_e}{v_0^{(q-1)/2}} \int w^{q-1} \Phi. \tag{3.9b}$$

To calculate $\psi(0)$ and $\eta(0)$, we need the following simple result, as proved in Lemma 3.1 of [22]:

Lemma 3.1 *(Lemma 3.1 of [22]) On $|x| < \ell$, suppose that $y(x)$ satisfies*

$$y_{xx} = 0, \quad -\ell < x < \ell; \qquad f_0 [y_x]_0 = f_1 y(0) + f_2; \qquad y(\ell) = zy(-\ell), \quad y_x(\ell) = zy_x(-\ell), \tag{3.10}$$

where f_0, f_1 and f_2, are nonzero constants, and let z satisfy (3.4). Then, $y(0)$ is given by

$$y(0) = f_2 \left[\frac{f_0}{\ell} \frac{(z-1)^2}{2z} - f_1 \right]^{-1} = -\frac{f_2}{f_0[1 - \cos(\pi j/K)]/\ell + f_1}. \tag{3.11}$$

Lemma 3.1 with $f_0 = e_0$, $f_1 = e_1$, and $f_2 = e_2\eta(0) + e_3$, yields $\psi(0)$ from (3.7). Similarly, $\eta(0)$ is found from (3.9) by using Lemma 3.1 with $f_0 = d_0$, $f_1 = d_1$, and $f_2 = d_2$. In this way, we get

$$\psi(0) = -\frac{e_2\eta(0) + e_3}{e_0[1 - \cos(\pi j/K)]/\ell + e_1}, \qquad \text{and} \qquad \eta(0) = -\frac{d_2}{d_0[1 - \cos(\pi j/K)]/\ell + d_1}. \tag{3.12}$$

Upon combining these two results, and using (3.7b) and (3.9b) for e_0 and d_0, respectively, we determine $\psi(0)$ as

$$\psi(0) = -\frac{1}{\mathcal{D}_j \alpha^2 + e_1} \left[e_3 - \frac{e_2 d_2}{\mathcal{D}_j \alpha^q + d_1} \right], \tag{3.13}$$

8

where we have defined $\mathcal{D}_j$, which satisfies $\mathcal{D}_j < \mathcal{D}_{j+1}$ for any $j = 0, \ldots, K-2$, by

$$\mathcal{D}_j \equiv \frac{\mathcal{D}}{\ell}\left[1 - \cos\left(\frac{\pi j}{K}\right)\right], \qquad j = 0, \ldots, K-1, \quad \text{where} \quad l = \frac{S}{2K}. \tag{3.14}$$

To determine the coefficient $\psi(0)/v_0^{3/2}$ in (3.5) in terms of the original parameters, which will yield the NLEP, we next need to simplify the expressions for e_1, e_2, e_3, d_1, and d_2 in (3.7b) and (3.9b), by using (2.6) for $\tilde{u}_e$ and an explicit formula for the integral ratio $\int w^{q+2}/\int w^q$, as given in (2.9). A short calculation yields that

$$e_1 = \frac{\int w^3}{v_0^{3/2}} + \frac{2qU_0}{(q+1)Kv_0}, \qquad e_2 = \frac{\int w^{q+2}}{v_0^{q/2}}, \qquad e_3 = 3\int w^2\Phi + \frac{U_0\sqrt{v_0}}{K}(q+2)\frac{\int w^{q+1}\Phi}{\int w^q}, \tag{3.15a}$$

$$d_1 = \hat{\tau}\lambda\frac{\int w^q}{v_0^{q/2}}, \qquad d_2 = \hat{\tau}\lambda q\left(\frac{U_0\sqrt{v_0}}{K}\right)\frac{\int w^{q-1}\Phi}{\int w^q}. \tag{3.15b}$$

Upon substituting (3.15) into (3.13), we obtain, after some algebra, that

$$-\frac{\psi(0)}{v_0^{3/2}} = \chi_{0j}\left(3\frac{\int w^2\Phi}{\int w^3}\right) + \chi_{1j}\left((q+2)\frac{\int w^{q+1}\Phi}{\int w^{q+2}}\right) + \chi_{2j}\left(q\frac{\int w^{q-1}\Phi}{\int w^q}\right), \tag{3.16a}$$

where we have defined

$$\chi_{0j} \equiv \frac{1}{1 + \kappa_q + v_0^{3/2}\mathcal{D}_j\alpha^2/\int w^3}, \qquad \chi_{1j} \equiv \chi_{0j}\kappa_q, \qquad \chi_{2j} \equiv -\chi_{0j}\left(\frac{\hat{\tau}\lambda\kappa_q}{\hat{\tau}\lambda + \mathcal{D}_j\alpha^q v_0^{q/2}/\int w^q}\right). \tag{3.16b}$$

Here κ_q is defined by

$$\kappa_q \equiv \frac{U_0\sqrt{v_0}}{K\int w^3}\frac{\int w^{q+2}}{\int w^q} = \frac{2qU_0}{[\omega(q+1)]}, \qquad \text{where} \qquad \omega \equiv S(\gamma - \alpha) - \frac{2qU_0}{q+1}. \tag{3.17}$$

In calculating κ_q above, we evaluated the integral ratio in (3.17) using (2.9) and then recalled (2.14) for v_0.

From (3.16b), we first derive the NLEP for the mode $j = 0$, which corresponds to synchronous perturbations of the hotspot amplitudes. For this mode, we have $\mathcal{D}_0 = 0$ from (3.14). Therefore, from (3.16b), the coefficients reduce to $\chi_{00} = 1/(1 + \kappa_q)$, $\chi_{10} = \kappa_q/(1 + \kappa_q)$, and $\chi_{20} = -\kappa_q/(1 + \kappa_q)$. With these values, we substitute (3.16a) into (3.5) to obtain the following NLEP for the synchronous mode:

Proposition 3.2 *For $\epsilon \to 0$, $K \geq 2$, $q > 1$, $0 < U_0 < U_{0,\max} = (q+1)S(\gamma - \alpha)/(2q)$, $\mathcal{D} = \epsilon^2 D = \mathcal{O}(1)$, and $\tau \ll \mathcal{O}(\varepsilon^{-2})$, the linear stability on an $\mathcal{O}(1)$ time-scale of a K-hotspot steady-state solution for (1.4) to synchronous perturbations of the hotspot amplitudes is determined by the spectrum of the following NLEP for $\Phi(y) \in L^2(\mathbb{R})$:*

$$L_0\Phi - \frac{w^3}{1 + \kappa_q}\left[3\frac{\int w^2\Phi}{\int w^3} + \kappa_q(q+2)\frac{\int w^{q+1}\Phi}{\int w^{q+2}} - \kappa_q q\frac{\int w^{q-1}\Phi}{\int w^q}\right] = \lambda\Phi, \tag{3.18}$$

where $L_0\Phi \equiv \Phi'' - \Phi + 3w^2\Phi$ and κ_q is defined by $\kappa_q = 2qU_0/[\omega(q+1)]$, where $\omega \equiv S(\gamma - \alpha) - 2qU_0/(q+1)$.

The NLEP (3.18) for the synchronous mode depends only on κ_q, and is independent of the criminal and police diffusivities.

Remark 3.3 *In §3.2 we show that the NLEP in (3.18) also governs the linear stability of a one-hotspot steady-state solution.*

Next we consider the asynchronous modes where $j = 1, \ldots, K - 1$. For these modes, in order to obtain an NLEP with as few bifurcation parameters as possible, we introduce in (3.16b) two additional rescaled parameters $\mathcal{D}_u$ and τ_u defined by

$$\mathcal{D}_j = \frac{\int w^3}{v_0^{3/2} \alpha^2} \mathcal{D}_u \,, \qquad \hat{\tau} = \mathcal{D}_j \alpha^q \frac{v_0^{q/2}}{\int w^q} \tau_u \,. \tag{3.19}$$

By using (3.19) in (3.16), an NLEP is obtained by substituting (3.16a) into (3.5). The result is summarized as follows.

Proposition 3.4 *For $\epsilon \to 0$, $K \geq 2$, $q > 1$, $0 < U_0 < U_{0,\max} = (q+1)S(\gamma - \alpha)/(2q)$, $\mathcal{D} = \epsilon^2 D = \mathcal{O}(1)$, and $\tau \ll \mathcal{O}(\varepsilon^{-2})$, the linear stability on an $\mathcal{O}(1)$ time-scale of a K-hotspot steady-state solution for (1.4) for the asynchronous modes $j = 1, \ldots, K - 1$ is characterized by the spectrum of the following NLEP for $\Phi(y) \in L^2(\mathbb{R})$:*

$$L_0 \Phi - \chi_0 w^3 \left(3 \frac{\int w^2 \Phi}{\int w^3} \right) - \chi_1 w^3 \left((q+2) \frac{\int w^{q+1} \Phi}{\int w^{q+2}} \right) - \chi_2 w^3 \left(q \frac{\int w^{q-1} \Phi}{\int w^q} \right) = \lambda \Phi \,, \tag{3.20a}$$

where $L_0 \Phi \equiv \Phi'' - \Phi + 3w^2 \Phi$ and $w = \sqrt{2} \operatorname{sech} y$ is the homoclinic of (2.4). Here the coefficients of the multipliers are

$$\chi_0 = \frac{1}{1 + \kappa_q + \mathcal{D}_u} \,, \quad \chi_1 = \chi_0 \kappa_q \,, \quad \chi_2 = -\chi_0 \kappa_q \frac{\tau_u \lambda}{1 + \tau_u \lambda} \,; \qquad \kappa_q = \frac{2q}{q+1} \frac{U_0}{\omega} \,, \quad \omega \equiv S(\gamma - \alpha) - \frac{2q}{q+1} U_0 \,. \tag{3.20b}$$

For a given $q > 1$, the spectrum of the NLEP (3.20) depends on the three key parameters $\mathcal{D}_u$, τ_u, and κ_q. To relate these parameters to the original criminal diffusivity $\mathcal{D}$ we use (3.19) and (3.14), and then (2.14) for v_0 to get

$$\mathcal{D} = \left(\frac{\int w^3}{\alpha^2 v_0^{3/2}} \right) \frac{S}{2K \left[1 - \cos\left(\frac{\pi j}{K}\right) \right]} \mathcal{D}_u = \frac{\omega^3 S}{4K^4 \pi^2 \alpha^2 \left[1 - \cos\left(\frac{\pi j}{K}\right) \right]} \mathcal{D}_u \,, \qquad j = 1, \ldots, K - 1 \,, \tag{3.21}$$

where ω is defined in (3.20b). In addition, to map τ_u to the original police diffusivity D_p, we simply substitute (3.19) for $\hat{\tau}$ into (3.8) for D_p and use (3.14) for $\mathcal{D}_j$ and (2.14) for v_0. In this way, we obtain

$$D_p = \frac{S \epsilon^{1-q} \int w^q}{2K \alpha^q \left[1 - \cos\left(\frac{\pi j}{K}\right) \right]} \left(\frac{\omega}{K \int w^3} \right)^q \left(\frac{1}{\tau_u} \right) \,, \qquad j = 1, \ldots, K - 1 \,. \tag{3.22}$$

We refer to the NLEP (3.20) as a *universal* NLEP, since we need only determine, with respect to the bifurcation parameters $\mathcal{D}_u$, τ_u and κ_q, when all discrete eigenvalues of (3.20) satisfy $\operatorname{Re}(\lambda) \leq 0$. The regions of linear stability with respect to these key parameters can then be mapped to corresponding regions of stability with respect to the original parameters $\mathcal{D}$ and D_p (for a given U_0, S, γ, α, and q) by using (3.21) and (3.22). Correspondingly, we will also identify parameter ranges for which the NLEP predicts instabilities owing to it having a discrete eigenvalue in $\operatorname{Re}(\lambda) > 0$.

3.2 Derivation of the NLEP for a Single Hotspot: $K = 1$ case

To derive an NLEP for the case of a single hotspot, we simply impose Neumann boundary conditions directly at $x = \pm \ell$ in (3.7) and (3.9). This yields that $\psi(x) = \psi(0)$ and $\eta(x) = \eta(0)$ on $|x| \leq \ell$. From (3.9) and (3.7), we conclude that

$$\eta(0) = -\frac{d_2}{d_1} \qquad \psi(0) = -\frac{1}{e_1} \left(e_2 \eta(0) + e_3 \right) = -\frac{1}{e_1} \left(e_3 - \frac{e_2 d_2}{d_1} \right) \,.$$

By using the explicit expressions for the coefficients given in (3.15), we calculate $\psi(0)/v_0^{3/2}$, which leads to the NLEP from (3.5). In this way, we obtain that the NLEP for a single hotspot is also given by (3.18) of Proposition 3.2.

10

4 No Unstable Eigenvalues for the NLEP (3.18)

In this section, we study the NLEP (3.18) of Proposition 3.2, which applies to either amplitude perturbations of a one-hotspot steady-state or synchronous perturbations of the amplitudes of a multi-hotspot steady-state.

4.1 Numerical Computations

We first show numerically that (3.18) has no unstable eigenvalues for any $\kappa_q \geq 0$ and $q > 1$. To do so, we write (3.18) as

$$L_0\Phi - w^3 \left(a \int w^{q+1}\Phi + b \int w^2\Phi + c \int w^{q-1}\Phi\right) = \lambda\Phi, \tag{4.1}$$

where the constants a, b, and c are defined by

$$a = \frac{\kappa_q(q+2)}{(1+\kappa_q)\int w^{q+2}}, \qquad b = \frac{3}{(1+\kappa_q)\int w^3}, \qquad c = -\frac{q\kappa_q}{(1+\kappa_q)\int w^q}. \tag{4.2}$$

To numerically compute the discrete eigenvalues of (4.1) we convert this NLEP into a linear algebra problem using finite differences. As we are interested only in even solutions, we consider (4.1) on $[0, \infty]$. Since $w(y)$ decays exponentially as $y \to +\infty$, we truncate the positive half-line to the large interval $x \in [0, L]$, where we chose $L = 20$ (decreasing L to 10 changes the results below by less than 0.01%). We discretize $\Phi(x_j) \sim \Phi_j$ where $x_j = j\Delta x$, for $j = 0 \ldots N-1$ and $\Delta x = L/(N-1)$, with $N = 100$. Increasing N to 200 changed the results below by less than 1%. We use standard centered differences to approximate Φ'' and the Trapezoid rule to approximate integrals in (4.1). In this way, we obtain the matrix eigenvalue problem $\mathcal{M}\boldsymbol{\Phi} = \lambda\boldsymbol{\Phi}$, where $\boldsymbol{\Phi} \equiv (\Phi_1, \ldots, \Phi_N)^T$. The eigenvalue of $\mathcal{M}$ with the largest real part then provides an excellent approximation to the principal eigenvalue of (4.1).
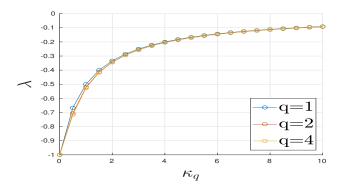

Figure 2: Numerical approximation of the principal eigenvalue of (4.1) for several values of q and with $\kappa \in (0, 10)$. We observe that $\lambda < 0$ in all cases, and that the principal eigenvalue is rather insensitive to changes in q.

In terms of κ_q this numerical approximation of the principal eigenvalue of (4.1) is plotted for $q = 1$, $q = 2$, and $q = 4$ in Fig. 2. The results shown in Fig. 2 suggests that (3.18) has no unstable eigenvalues for any $\kappa_q \geq 0$ and $q \geq 1$. Although the NLEP (3.18) is relevant to the stability of a hotspot steady-state only when $q > 1$, as a partial confirmation of the numerical results in Fig. 2 we now show how to determine λ analytically from (4.1) when $q = 1$.

Let Φ and λ be any eigenpair of (4.1) for which $\int w^2\Phi \neq 0$ and $\int \Phi \neq 0$. We multiply (4.1) by w^2 and integrate. By using the identity $L_0w^2 = 3w^2$, we obtain

$$(\lambda - 3)\int w^2\Phi = -(a+b)\int w^5\int w^2\Phi - c\int w^5\int \Phi. \tag{4.3}$$

Next, we integrate (4.1) upon recalling $L_0\Phi = \Phi'' - \Phi + 3w^2\Phi$. This yields

$$(\lambda + 1)\int \Phi = 3\int w^2\Phi - \int w^3 \left[(a + b)\int w^2\Phi + c\int \Phi\right]. \tag{4.4}$$

By eliminating $\int \Phi w^2$ and $\int \Phi$ from (4.3) and (4.4), we then obtain the following quadratic equation for λ:

$$c\int w^5\left(3 - (a + b)\int w^3\right) + \left(\lambda - 3 + (a + b)\int w^5\right)\left(c\int w^3 + \lambda + 1\right) = 0. \tag{4.5}$$

For $q = 1$, we obtain from (4.2) that $a + b = 3/\int w^3$, and $c = -\kappa_1/\left[(1 + \kappa_1)\int w\right]$. Upon substituting these expressions into (4.5), and using $\int w^3/\int w = 1$ and $\int w^5/\int w^3 = 3/2$, we get

$$\left(\lambda + \frac{1}{1 + \kappa_1}\right)\left(\lambda + \frac{3}{2}\right) = 0. \tag{4.6}$$

Since $\kappa_1 \geq 0$, we conclude that the principal eigenvalue of (4.1) when $q = 1$ is

$$\lambda = -\frac{1}{1 + \kappa_1}. \tag{4.7}$$

Setting $\kappa_1 = 1$ gives $\lambda = -1/2$, which agrees with the numerical result shown in Fig. 2 arising from a discretization of (4.1).

4.2 Hybrid Analytical-Numerical Approach $q \neq 2$

We now give an alternative approach that provides a sufficient condition to ensure that the NLEP (3.18) has no unstable eigenvalues. This sufficient condition is then investigated numerically. For this hybrid analytical-numerical approach, we write the NLEP (3.18) in the alternative form

$$L_0\Phi - 2w^3\frac{\int f(w)\Phi}{\int w^3} = \lambda\Phi, \tag{4.8a}$$

where $L_0\Phi \equiv \Phi'' - \Phi + 3w^2\Phi$, and $f(w)$ is defined by

$$f(w) \equiv \frac{3}{2(1 + \kappa_q)}w^2 + \frac{(q + 2)\kappa_q}{2(1 + \kappa_q)}w^{q+1}\frac{\int w^3}{\int w^{q+2}} - \frac{q\kappa_q}{2(1 + \kappa_q)}w^{q-1}\frac{\int w^3}{\int w^q}. \tag{4.8b}$$

When $\kappa_q = 0$, where $f(w) = 3w^2/2$, the NLEP (4.8a) has no unstable eigenvalues by Theorem 1 of [25] (see also Lemma 3.2 of [11]).

We multiply (4.8a) by $\bar{\Phi}$ and integrate over the real line. Upon integrating by parts and taking the real part we get

$$I_k[\Phi_R] + I_k[\Phi_I] = -\lambda_R\int|\Phi|^2, \tag{4.9}$$

where $\Phi = \Phi_R + i\Phi_I$ and $\lambda = \lambda_R + i\lambda_I$. Here the quadratic form is defined by

$$I_k[\Phi] \equiv \int (\Phi')^2 + \Phi^2 - 3w^2\Phi^2 + 2\frac{\int w^3\Phi\int f(w)\Phi}{\int w^3}. \tag{4.10}$$

To show that $\lambda_R < 0$, so that there are no unstable eigenvalues of the NLEP (4.8), it is sufficient to show that the quadratic form $I_k[\Phi]$ is positive definite. In Appendix C we establish the following lemma for $I_0[\Phi]$.

Lemma 4.1 *We have $I_0[\Phi] > 0 \ \ \forall\Phi \not\equiv 0$.*

12

Since $I_0[\Phi] > 0$, our strategy is to continue in $\kappa_q > 0$ until we reach a point for which $I_k[\Phi]$ ceases to be positive definite. To analyze this transition, we observe that $I_k[\Phi] = \int -\Phi \mathcal{L}\Phi$, where $\mathcal{L}\Phi$ is the linear operator

$$\mathcal{L}\Phi \equiv L_0\Phi - \frac{\int f(w)\Phi}{\int w^3}w^3 - \frac{\int w^3\Phi}{\int w^3}f(w)\,. \tag{4.11}$$

Since $\mathcal{L}$ is self-adjoint, it follows that $I_k[\Phi]$ is positive definite if and only if $\mathcal{L}$ has only negative eigenvalues. This motivates the consideration of the following zero-eigenvalue problem for $\mathcal{L}$:

$$\mathcal{L}\Phi = 0\,, \qquad \Phi \in L^2(\mathbb{R})\,, \qquad \Phi \not\equiv 0\,. \tag{4.12}$$

To analyze (4.12) we use (4.11) to get

$$\Phi = \frac{\int f(w)\Phi}{\int w^3}L_0^{-1}w^3 + \frac{\int w^3\Phi}{\int w^3}L_0^{-1}f(w)\,. \tag{4.13}$$

Define $c_1 = \int f(w)\Phi$ and $c_2 = \int w^3\Phi$. By multiplying (4.13) by $f(w)$ and then by w^3 we get the linear system

$$c_1 = c_1\frac{\int f(w)L_0^{-1}w^3}{\int w^3} + c_2\frac{\int f(w)L_0^{-1}f(w)}{\int w^3}\,, \qquad c_2 = c_1\frac{\int w^3 L_0^{-1}w^3}{\int w^3} + c_2\frac{\int w^3 L_0^{-1}f(w)}{\int w^3}\,. \tag{4.14}$$

Upon using $L_0^{-1}w^3 = w/2$, and integrating by parts, we obtain that (4.14) has a nontrivial solution iff $g(\kappa_q) = 0$, where

$$g(\kappa_q) \equiv \det\begin{pmatrix} \frac{\int wf(w)}{2\int w^3} - 1 & \frac{\int f(w)L_0^{-1}f(w)}{\int w^3} \\ \frac{\int w^4}{2\int w^3} & \frac{\int wf(w)}{2\int w^3} - 1 \end{pmatrix} = \left(\frac{\int wf(w)}{2\int w^3} - 1\right)^2 - \frac{\int w^4}{2\left(\int w^3\right)^2}\int f(w)L_0^{-1}f(w)\,. \tag{4.15}$$

When $\kappa_q = 0$, we have $f(w) = 3w^2/2$. Upon using $L_0^{-1}w^2 = w^2/3$, $\int w^4 = 16/3$, and $\int w^3 = \sqrt{2}\pi$, we calculate

$$g(0) = \frac{1}{16} - \frac{16}{3\pi^2} < 0\,. \tag{4.16}$$

Thus, when $\kappa_q = 0$, the only solution to (4.14) is $c_1 = c_2 = 0$, and so (4.11) becomes $L_0\Phi = 0$, which has no nontrivial even solution. By increasing κ_q, we conclude that a sufficient condition for guaranteeing no unstable eigenvalues of the NLEP (4.8) is that on the range $0 < \kappa_q < \kappa_{q0}$ we have $g(\kappa_q) < 0$. Here κ_{q0} is defined by

$$\kappa_{q0} = \sup\{\kappa_q \mid g(t) < 0\,, \ t \in (0, \kappa_q)\}\,. \tag{4.17}$$

In Fig. 3 we plot $g(\kappa_q)$ versus κ_q for $q = 2, 3, 4$. These results were obtained by numerically evaluating the integrals in (4.15), after computing $L_0^{-1}f(w)$ from a BVP solver. On the range for which $g(\kappa_q) < 0$, we conclude that $I_k[\Phi]$ is positive definite so that the NLEP (4.8) has no unstable eigenvalues.

As a partial confirmation of the results in Fig. 3 we now show how to calculate $g(\kappa_q)$ analytically when $q = 2$. When $q = 2$, we have that $\psi \equiv L_0^{-1}f$ satisfies

$$L_0\psi = f\,, \qquad f = e_0 w^2 + e_1 w^3 + e_2 w\,, \tag{4.18a}$$

where e_0, e_1, and e_2, are defined by

$$e_0 = \frac{3}{2(1 + \kappa_2)}\,, \qquad e_1 = \frac{2\kappa_2}{1 + \kappa_2}\frac{\int w^3}{\int w^4}\,, \qquad e_2 = -\frac{\kappa_2}{1 + \kappa_2}\frac{\int w^3}{\int w^2}\,. \tag{4.18b}$$

By using (4.18a) for $f(w)$, we calculate

$$\frac{\int wf(w)}{2\int w^3} - 1 = \frac{3}{4(1 + \kappa_2)} + \frac{\kappa_2}{2(1 + \kappa_2)} - 1 = -\frac{(1 + 2\kappa_2)}{4(1 + \kappa_2)}\,. \tag{4.19}$$
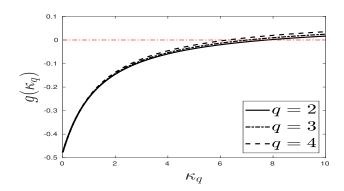
13

Figure 3: *Plot of numerically computed $g(\kappa_q)$ versus κ_q, as defined in (4.15), for $q = 2, 3, 4$. For $q = 2$, $g(\kappa_2)$ is given analytically in (4.22). On the range of κ_q for which $g(\kappa_q) < 0$, the NLEP (4.8) has no unstable eigenvalues.*

Next, upon using $L_0 w^2 = 3w^2$, $L_0 w = 2w^3$ and $L_0(w + yw') = 2w$, we calculate from (4.18a) that

$$\psi \equiv L_0^{-1} f = \frac{e_0}{3} w^2 + \frac{e_1}{2} w + \frac{e_2}{2} (w + yw') \,. \tag{4.20}$$

Upon using (4.20) and (4.18b), we obtain after some rather lengthy, but straightforward, algebra that

$$\frac{\int w^4}{2 \left(\int w^3 \right)^2} \int f L_0^{-1} f = \frac{\kappa_2^2}{2(1 + \kappa_2)^2} - \frac{1}{4(1 + \kappa_2)^2} \left(\kappa_2^2 + 2\kappa_2 \right) \frac{\int w^4}{\int w^2} + \frac{3}{8(1 + \kappa_2)^2} \left(\frac{\int w^4}{\int w^3} \right)^2 + \frac{\kappa_2}{(1 + \kappa_2)^2} \left[\frac{3}{4} + \frac{\int w^5}{2 \int w^3} \right] \,. \tag{4.21}$$

We then simply the expression in (4.21) by using $\int w^4 = 16/3$, $\int w^2 = 4$, $\int w^3 = \sqrt{2}\pi$ and $\int w^5 = 3\sqrt{2}\pi/2$. In this way, and by combining the resulting expression with (4.19), we obtain from (4.15) that

$$g(\kappa_2) = \frac{1}{16(1 + \kappa_2)^2} \left[(2\kappa_2 + 1)^2 - \frac{8}{3} \left(\kappa_2^2 + 5\kappa_2 + \frac{32}{\pi^2} \right) \right] \,. \tag{4.22}$$

Recalling the definition of the threshold κ_{20} in (4.17), a simple calculation using (4.22) yields $\kappa_{20} = \frac{1}{2} \left[7 + \sqrt{46 + 256/\pi^2} \right] \approx 7.74$. The formula for $g(\kappa_2)$ in (4.22), and the threshold κ_{20}, agrees with the numerical results shown in Fig. 3.

In summary, we have shown that whenever $g(\kappa_q) < 0$ in (4.15), the NLEP (4.8) has no unstable eigenvalues. This sufficient condition for stability was implemented numerically for $q \neq 2$, and analytically for $q = 2$, which showed that the NLEP has no unstable eigenvalues for κ_q below some threshold. On the other hand, the numerical results in Fig. 2 obtained from a finite-difference approximation suggested that the NLEP (4.8) has no unstable eigenvalues *for all $\kappa_q > 0$*.

4.2.1 No Unstable Eigenvalues for $q = 2$ and any κ_2

In this subsection we provide a different approach to prove that for $q = 2$ that there are no instabilities associated with synchronous perturbations of the hotspot amplitudes *for any $\kappa_2 > 0$*. For $q = 2$, this NLEP has the general form

$$L_0 \Phi - w^3 \left[a \int w^3 \Phi + b \int w^2 \Phi + c \int w \Phi \right] = \lambda \Phi \,, \qquad \Phi \in L^2(\mathbb{R}) \,; \qquad L_0 \Phi \equiv \Phi'' - \Phi + 3w^2 \Phi \,. \tag{4.23}$$

We will convert this NLEP into one with a single nonlocal term proportional to $\int w \Phi$ by using the two identities (cf. [22]):

$$L_0 w = 2w^3 \,, \qquad L_0(w^2) = 3(w^2) \,. \tag{4.24}$$

Let Φ and λ be any eigenpair of (4.23). We first multiply (4.23) by w, and then use the first of (4.24), together with Green's identity, to obtain

$$\int w L_0 \Phi = \int \Phi L_0 w = 2 \int w^3 \Phi = a \int w^4 \int w^3 \Phi + b \int w^4 \int w^2 \Phi + c \int w^4 \int w \Phi + \lambda \int w \Phi \,. \tag{4.25a}$$

14

Next, we multiply (4.23) by w^2, and then use the second of (4.24), together with Green's identity, to obtain

$$\int w^2 L_0 \Phi = \int \Phi L_0 w^2 = 3 \int w^2 \Phi = a \int w^5 \int w^3 \Phi + b \int w^5 \int w^2 \Phi + c \int w^5 \int w \Phi + \lambda \int w^2 \Phi. \qquad (4.25\text{b})$$

Equations (4.25a) and (4.25b) provide a matrix system for $\int w^2 \Phi$ and $\int w^3 \Phi$ of the form

$$\begin{pmatrix} 3 - \lambda - b \int w^5 & -a \int w^5 \\ b \int w^4 & a \int w^4 - 2 \end{pmatrix} \begin{pmatrix} \int w^2 \Phi \\ \int w^3 \Phi \end{pmatrix} = \begin{pmatrix} c \int w^5 \\ -\left(\lambda + c \int w^4\right) \end{pmatrix} \int w \Phi. \qquad (4.26)$$

By inverting the matrix in (4.26), we obtain that

$$\int w^2 \Phi = \frac{-(2c + a\lambda) \int w^5}{(3 - \lambda)\left(a \int w^4 - 2\right) + 2b \int w^5} \int w \Phi, \qquad \int w^3 \Phi = \frac{-\left(\lambda + c \int w^4\right)(3 - \lambda) + b\lambda \int w^5}{(3 - \lambda)\left(a \int w^4 - 2\right) + 2b \int w^5} \int w \Phi, \qquad (4.27)$$

provided that

$$(3 - \lambda)\left(a \int w^4 - 2\right) + 2b \int w^5 \neq 0. \qquad (4.28)$$

By substituting (4.27) into (4.23), and using $\int w^2 = 4$, we obtain after some algebra the following NLEP with a single nonlocal term:

$$L_0 \Phi - 2w^3 \gamma \frac{\int w \Phi}{\int w^2} = \lambda \Phi, \qquad \text{where} \qquad \gamma = \frac{2(3 - \lambda)(a\lambda + 2c)}{(\lambda - 3)\left(a \int w^4 - 2\right) - 2b \int w^5}. \qquad (4.29)$$

Conversely, suppose that Φ and λ is any eigenpair of (4.29). Upon multiplying (4.29) by w, and then by w^2, and using (4.24), we obtain from (4.29) that

$$(3 - \lambda) \int w^2 \Phi = 2\gamma \frac{\int w^5}{\int w^2} \int w \Phi, \qquad 2 \int w^3 \Phi = \left(2\gamma \frac{\int w^4}{\int w^2} + \lambda\right) \int w \Phi. \qquad (4.30)$$

Next, by adding and subtracting terms in (4.29) we get

$$L_0 \Phi - w^3 \left[a \int w^3 \Phi + b \int w^2 \Phi + c \int w \Phi + \xi\right] = \lambda \Phi, \qquad \xi \equiv \left(\frac{2\gamma}{\int w^2} - c\right) \int w \Phi - b \int w^2 \Phi - a \int w^3 \Phi, \qquad (4.31)$$

which reduces to (4.23) only when $\xi = 0$. We solve (4.30) for $\int w^3 \Phi$, and for $\int w^2 \Phi$ which requires $\lambda \neq 3$. Then, upon using (4.29) for γ, we can readily verify from (4.31) that $\zeta = 0$. Therefore, any eignpair of (4.29) with $\lambda \neq 3$ is also an eigenpair of (4.23).

For $q = 2$, the coefficients a, b, and c in (4.2) associated with synchronous perturbations of the hotspot amplitudes are

$$a = \frac{4\kappa}{(1 + \kappa) \int w^4}, \qquad b = \frac{3}{(1 + \kappa) \int w^3}, \qquad c = -\frac{2\kappa}{(1 + \kappa) \int w^2}, \qquad (4.32)$$

where we label $\kappa \equiv \kappa_2$. By combining (4.32) and (4.29), and using $\int w^4 / \int w^2 = 4/3$ and $\int w^5 / \int w^3 = 3/2$, we get

$$\gamma = \frac{\kappa(3 - \lambda)(3\lambda - 4)}{2\left[2(\lambda - 3)(\kappa - 1) - 9\right]}, \qquad (4.33)$$

while the condition (4.28) becomes $(\lambda - 3)(\kappa - 1) \neq 9/2$.

To prove that (4.29), with γ as in (4.33), has no unstable eigenvalues we will use a key inequality that can readily be derived by proceeding as in (2.22) of [26] (see also equation (2.27) in §2 of [24]). Suppose that (4.29) has an eigenvalue with $\text{Re}(\lambda) \geq 0$. Then, the following inequality must hold:

$$\mathcal{T} \equiv 2 \left(\frac{\int w^4}{\int w^2}\right) |\gamma - 1|^2 + \text{Re}\left[\bar{\lambda}(\gamma - 1)\right] \leq 0, \qquad (4.34)$$

15

where the bars denote modulus. From (4.33), we calculate that

$$\gamma - 1 = \frac{-3\lambda^2\kappa + \lambda(9\kappa + 4) + 6}{4(\kappa - 1)\lambda - 12\kappa - 6}.$$
(4.35)

We will now use (4.34), with (4.35), to show that the NLEP (4.29) cannot have any purely complex eigenvalues of the form $\lambda = i\omega$. For $\lambda = i\omega$, we write $\gamma - 1$ in (4.35) as

$$\gamma - 1 = \frac{z_1}{z_2}, \qquad z_1 = 6 + 3\omega^2\kappa + i\omega(9\kappa + 4), \qquad z_2 = -6(1 + 2\kappa) + 4i\omega(\kappa - 1).$$
(4.36)

Using $\int w^4 / \int w^2 = 4/3$, we calculate from (4.34) that

$$\mathcal{T} = \frac{8}{3}\frac{|z_1|^2}{|z_2|^2} + \mathrm{Re}\left(-i\omega\frac{z_1}{z_2}\right) = \frac{8}{3}\frac{|z_1|^2}{|z_2|^2} - \mathrm{Re}\left(\frac{i\omega z_1 \bar{z}_2}{|z_2|^2}\right) = \frac{1}{3|z_2|^2}\left[8|z_1|^2 + 3\omega\mathrm{Im}\left(z_1\bar{z}_2\right)\right].$$
(4.37)

Upon substituting (4.36) into (4.37), we obtain after some rather lengthy, but straightforward, algebra that

$$\mathcal{T} = \frac{12}{36(1 + 2\kappa)^2 + 16\omega^2(\kappa - 1)^2}\left[\kappa(\kappa + 1)\omega^4 + \frac{\omega^2}{18}\left(162\kappa^2 + 243\kappa + 64\right) + 8\right].$$
(4.38)

This shows that $\mathcal{T} > 0$ holds $\forall \kappa > 0$ and ω. From our key inequality (4.34), it follows that the NLEP (4.29) does not undergo a Hopf bifurcation for any $\kappa \geq 0$.

To conclude the analysis of linear stability we use a continuation argument in κ. With a, b, and c as given in (4.32), the NLEP (4.23) has no unstable eigenvalues when $\kappa = 0$ by Theorem 1 of [25] (see also Lemma 3.2 of [11]). By our established correspondence between the two NLEPs (4.23) and (4.29), this linear stability result can also be seen from (4.29), as (4.29) has no unstable eigenvalues with $\lambda \neq 3$ when $\kappa = 0$. This latter result is immediate since when $\kappa = 0$, we have $\gamma = 0$ in (4.29). Therefore, (4.29) reduces to $L_0\Phi = \lambda\Phi$, which has no unstable eigenvalues with $\lambda \neq 3$ (cf. [7]).

Next, if we continue in κ, we claim that all eigenvalues of (4.23) must remain in the stable left half-plane $\mathrm{Re}(\lambda) \leq 0$. We establish this by contradiction. Suppose that at some point, $\kappa = \kappa_0 > 0$, an eigenvalue crosses the imaginary axis, i.e. it satisfies $\mathrm{Re}(\lambda) = 0$. At this point κ_0, and for this purely complex eigenvalue, it follows that $\lambda(k - 1) \neq 9/2$ and so the restriction (4.28) holds. Therefore, this eigenvalue must satisfy the NLEP (4.29) with only one nonlocal term. Our proof above that the NLEP (4.29) has no purely imaginary eigenvalue provides the required contradiction.

5 Analysis of the NLEP: Competition Instability

In this section we will analyze zero-eigenvalue crossings for the NLEP (3.20), corresponding to asynchronous perturbations of the hotspot amplitudes. This zero-eigenvalue crossing will yield $K - 1$ critical values of the criminal diffusivity $\mathcal{D}$. We will determine the behavior of this stability threshold in terms of the police focus parameter q and policing level U_0.

By using $L_0 w = 2w^3$, and noting that $\chi_2 = 0$ when $\lambda = 0$, it follows that (3.20) has a zero eigenvalue when

$$2 = 3\chi_0 + (q + 2)\chi_1,$$
(5.1)

for which $\Phi = w$. By using (3.20b) for χ_0 and χ_1, we solve (5.1) for $\mathcal{D}_u$ to conclude that the NLEP (3.20) has a zero eigenvalue at the critical value of $\mathcal{D}_u$ given by

$$\mathcal{D}_u = \frac{1}{2}\left(1 + q\kappa_q\right), \qquad \text{where} \qquad \kappa_q = \frac{2q}{q + 1}\frac{U_0}{\omega}.$$
(5.2)

Then, by using (3.21), it follows that a zero-eigenvalue crossing occurs at $\mathcal{D} = \mathcal{D}_j$, for $j = 1, \ldots, K - 1$, given by

$$\mathcal{D}_j = \frac{S}{8K^4\pi^2\alpha^2\left[1 - \cos\left(\frac{\pi j}{K}\right)\right]}\left[\omega^3 + \frac{2q^2 U_0}{q + 1}\omega^2\right], \qquad j = 1, \ldots, K - 1.$$
(5.3)

The smallest such threshold $\mathcal{D}_c = \min_j \mathcal{D}_j$ on $j = 1, \ldots, K - 1$, referred to as the competition stability threshold, occurs when $j = K - 1$. We write $\mathcal{D}_c$ as

$$\mathcal{D}_c \equiv \mathcal{D}_{K-1} = \frac{S}{8K^4\pi^2\alpha^2\left[1 + \cos\left(\pi/K\right)\right]}g(U_0; q), \tag{5.4a}$$

where $g(U_0; q)$ is defined on the range $0 \leq U_0 < U_{0,\max} = S(\gamma - \alpha)(q + 1)/(2q)$ by

$$g(U_0; q) \equiv \omega^3 + \left(\frac{2q^2}{q+1}U_0\right)\omega^2 = (1 - q)\omega^3 + qS(\gamma - \alpha)\omega^2, \qquad \text{where} \qquad \omega = S(\gamma - \alpha) - 2qU_0/(q + 1). \tag{5.4b}$$

For a general value of $q > 1$, owing to the presence of the three distinct nonlocal terms in (3.20), it is analytically intractable to perform a full linear stability analysis of hotspot steady-states on either side of the zero-eigenvalue crossing value $\mathcal{D} = \mathcal{D}_c$. For the specific $q = 2$ "cops-on-the-dots" case, where some key identities can be used to reduce (3.20) to an NLEP with only one nonlocal term, this linear stability problem is studied in §6 by using a hybrid analytical-numerical approach. However, for a general $q > 1$, in §5.1 we show analytically that the NLEP (3.20) always has a unique unstable eigenvalue in $\mathrm{Re}(\lambda) > 0$ whenever $\mathcal{D} > \mathcal{D}_c$ and $\tau_u = 0$, and has no unstable eigenvalue when $\mathcal{D} < \mathcal{D}_c$. This partial result proves that, for an infinite police diffusivity, the hotspot steady-state is always unstable for any $q > 1$ when $\mathcal{D}$ exceeds $\mathcal{D}_c$.

In the remainder of this sub-section, we examine how the competition stability threshold $\mathcal{D}_c$ depends on the degree q of patrol focus and the level U_0 of police deployment. From (2.12), the maximum $A_{\max}$ of the steady-state attractiveness field is $A_{\max} \sim \epsilon^{-1}\omega/(K\pi)$, which decreases as either ω decreases or as K increases. From Corollary 2.2, we observe that the criminal density ρ at the hotspot locations is $\rho_{\max} = [w(0)]^2 = 2$, which is independent of q and U_0, with $\rho = \mathcal{O}(\epsilon^2)$ away from the hotspot regions. As a result, the total crime is reduced primarily by decreasing the number of stable steady-state hotspots on the given domain. As such, we seek to tune the police parameters q and U_0 so that the range of diffusivity $\mathcal{D}$ for which a K-hotspot steady-state is unstable when $\tau_u = 0$ (see §5.1 below) is as large as possible. This corresponds to minimizing the competition stability threshold $\mathcal{D}_c$ in (5.4), which is determined in terms of $g(U_0; q)$ in (5.4b).

We first fix $q > 1$, and study how $g(U_0; q)$ depends on U_0. On $0 < U_0 < U_{0,\max} \equiv S(\gamma - \alpha)(q + 1)/(2q)$, we find that

$$\frac{dg}{dU_0} = -\frac{2q}{q+1}\left[\frac{6q(q-1)}{q+1}U_0 + (3 - q)S(\gamma - \alpha)\right]. \tag{5.5}$$

This shows that $dg/dU_0 < 0$ on $0 < U_0 < U_{0,\max}$ whenever $1 < q < 3$. Thus, when the patrol is not too focused, i.e. when $1 < q < 3$, increasing the overall policing level leads to a larger range of $\mathcal{D}$ where the hotspot steady-state is unstable when $\tau_u = 0$. For $q > 3$, (5.5) also yields that

$$\frac{dg}{dU_0} > 0 \quad \text{on} \quad 0 < U_0 < S(\gamma - \alpha)\left(\frac{q - 3}{3(q - 1)}\right) < U_{0,\max}; \qquad \frac{dg}{dU_0} < 0 \quad \text{on} \quad S(\gamma - \alpha)\left(\frac{q - 3}{3(q - 1)}\right) < U_0 < U_{0,\max}. \tag{5.6}$$

Therefore, with an overly focused police patrol (i.e. $q > 3$), the hotspot steady-state is destabilized only by having a sufficiently large policing level. This is illustrated in Fig. 4 where we plot $g(U_0; q)$ versus U_0 for several values of q.

Next, we fix U_0 in $0 < U_0 < U_{0,\max}$ and determine how $g(U_0; q)$ depends on q for $q > 1$. We readily calculate that

$$\frac{dg}{dq} = \frac{2\omega U_0}{(q+1)^3}\left[\omega(q + 3)(q^2 - 1) - 4q^2 U_0\right], \qquad \text{where} \quad \omega \equiv S(\gamma - \alpha) - 2qU_0/(q + 1). \tag{5.7}$$

This shows that $dg/dq < 0$ if $0 < \omega < 4q^2 U_0/[(q + 3)(q^2 - 1)]$. By relating ω to U_0, this inequality yields

$$\frac{dg}{dq} < 0 \quad \text{when} \quad U_{0,\max}\left[1 + \frac{2q}{(q + 3)(q - 1)}\right]^{-1} < U_0 < U_{0,\max}. \tag{5.8}$$

The qualitative interpretation of this result is that if the policing level is sufficiently close to its maximum value $U_{0,\max}$, an increase in the patrol focus parameter q yields a larger range in $\mathcal{D}$ where the hotspot steady-state is unstable when $\tau_u = 0$.
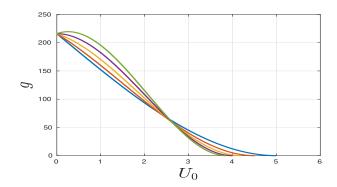
Figure 4: Competition stability threshold nonlinearity $g(U_0; q)$, as defined in (5.4b), versus U_0 on the range $0 < U_0 < U_{0,\max} \equiv S(\gamma - \alpha)(q+1)/(2q)$ for $q = 1.5, 2.0, 2.5, 3.0, 3.5$, when $S = 6$, $\gamma = 2$, and $\alpha = 1$. Smaller values of q correspond to larger values of $U_{0,\max}$. Notice that g is not monotone in U_0 when $q > 3$. From (5.4), the competition threshold $\mathcal{D}_c$ is a positive scaling of $g(U_0; q)$.

5.1 Infinite Police Diffusivity: An Instability Result for $\mathcal{D} > \mathcal{D}_c$

When $\tau_u = 0$, we now prove that the NLEP (3.20), corresponding to asynchronous perturbations of the amplitudes of the steady-state hotspot pattern, has an unstable positive real eigenvalue whenever $\mathcal{D}_u > \frac{1}{2}(1 + q\kappa_q)$. This will establish that a multi-hotspot steady-state is unstable for an infinite police diffusivity whenever $\mathcal{D}$ exceeds the competition stability threshold $\mathcal{D}_c$ defined in (5.4). When $\tau_u = 0$, we have $\chi_2 = 0$ and so (3.20) reduces to an NLEP with two nonlocal terms

$$L_0\Phi - \chi_0 w^3 \left(3\frac{\int w^2 \Phi}{\int w^3} \right) - \chi_1 w^3 \left((q+2)\frac{\int w^{q+1}\Phi}{\int w^{q+2}} \right) = \lambda\Phi, \qquad \text{where} \qquad \chi_0 = \frac{1}{(1 + \kappa_q + \mathcal{D}_u)}, \quad \chi_1 = \chi_0\kappa_q. \qquad (5.9)$$

To analyze (5.9), we first reformulate it into an NLEP with only one nonlocal term by using the key identity $L_0(w^2) = 3(w^2)$ (cf. [22]). Upon multiplying (5.9) by w^2, and then using Green's identity, we readily calculate that

$$\int w^2 \Phi \left(3 - 3\chi_0 \frac{\int w^5}{\int w^3} - \lambda \right) = \chi_1(q+2) \left(\frac{\int w^5}{\int w^{q+2}} \right) \int w^{q+1}\Phi. \qquad (5.10)$$

Since $\int w^5 / \int w^3 = 3/2$ from (2.5), (5.10) yields that

$$\int w^2\Phi = \left(\frac{\chi_1(q+2)\int w^5}{3 - \frac{9\chi_0}{2} - \lambda} \right) \frac{\int w^{q+1}\Phi}{\int w^{q+2}}, \qquad (5.11)$$

provided that $\lambda \neq 3 - 9\chi_0/2$. Then, by substituting (5.11) back into (5.9), and using $\chi_1 = \chi_0\kappa_q$, we obtain the following equivalent NLEP with only one nonlocal term (provided that $\lambda \neq 3 - 9\chi_0/2$):

$$L_0\Phi - \chi_c(\lambda)w^3 \frac{\int w^{q+1}\Phi}{\int w^{q+2}} = \lambda\Phi, \qquad \text{where} \qquad \chi_c(\lambda) \equiv \chi_0\kappa_q(q+2)\left(\frac{3 - \lambda}{3 - \frac{9\chi_0}{2} - \lambda} \right). \qquad (5.12)$$

To interpret the apparent restriction that $\lambda \neq 3 - 9\chi_0/2$, we observe that since $\chi_1 = \chi_0\kappa_q$ is proportional to U_0 (see (3.20b) for the definition of κ_q), it follows from (5.10) that for any eigenpair for which $\int w^{q+1}\Phi \neq 0$ for any $q > 1$, we must have $\lambda = 3 - 9\chi_{0,j}/2$ if and only if $U_0 = 0$. For the case of no police, this recovers the result in equation (3.17) of [11] for the unique discrete eigenvalue of the linearization of a K-hotspot steady-state of the basic two-component crime model.

We now show that the reformulated NLEP (5.12) has an unstable real eigenvalue whenever $\mathcal{D}_u > \frac{1}{2}(1 + q\kappa_q)$. To do so, we convert (5.12) into a root-finding problem. We write $\Phi = \chi_c (L_0 - \lambda)^{-1} w^3 \int w^{q+1}\Phi / \int w^{q+2}$, multiply both sides by w^{q+1}, and then integrate over the real line. In this way, and by using (5.9) for χ_0, we readily find that any discrete

eigenvalue of (5.12) in $\text{Re}(\lambda) > 0$ must be a root of $\zeta(\lambda) = 0$ defined by

$$\zeta(\lambda) \equiv \mathcal{C}_c(\lambda) - \mathcal{F}(\lambda),\tag{5.13a}$$

where

$$\mathcal{C}_c(\lambda) \equiv \frac{1}{\chi_c(\lambda)} = \frac{(1 + \kappa_q + \mathcal{D}_u)}{\kappa_q(q+2)} + \frac{9}{2\kappa_q(q+2)(\lambda-3)}, \qquad \text{and} \qquad \mathcal{F}(\lambda) \equiv \frac{\int w^{q+1}\left(L_0 - \lambda\right)^{-1} w^3}{\int w^{q+2}}.\tag{5.13b}$$

When $\mathcal{D}_u > \frac{1}{2}\left(1 + q\kappa_q\right)$, we claim that $\zeta(\lambda) = 0$ has a real root in $0 < \lambda < 3$, which yields an unstable eigenvalue for the NLEP (5.12). To show this, we use $L_0 w = 2w^3$ to calculate $\mathcal{F}(0) = \int w^{q+1} L_0^{-1}(w^3)/\int w^{q+2} = 1/2$, and observe that $\mathcal{F}(\lambda) \to +\infty$ as $\lambda \to \nu_0^-$, where $\nu_0 = 3$ is the unique positive eigenvalue of L_0 (cf. [7], [22]). Moreover, we observe that

$$\mathcal{C}_c(\lambda) \to -\infty \quad \text{as} \quad \lambda \to 3^-, \qquad \text{and} \qquad \mathcal{C}_c(0) = \frac{(\kappa_q + \mathcal{D}_u - 1/2)}{\kappa_q(q+2)},$$

which yields that $\mathcal{C}_c(0) > 1/2$ when $\mathcal{D}_u > \frac{1}{2}\left(1 + q\kappa_q\right)$. With these properties of $\mathcal{C}_c(\lambda)$ and $\mathcal{F}(\lambda)$, it follows from the intermediate value theorem that $\zeta(\lambda)$ has a root at some value of λ on $0 < \lambda < 3$.

This simple result proves that a multi-hotspot steady-state is unstable for $\tau_u = 0$, i.e. for an infinite police diffusivity, whenever $\mathcal{D}$ exceeds the competition stability threshold $\mathcal{D}_c$ in (5.4).

Next, by using a winding number criterion, we now obtain a more precise result for the spectrum of the NLEP (5.12), which pertains to the special case $\tau_u = 0$. We do so by determining the number N of zeroes of $\zeta(\lambda)$ in $\text{Re}(\lambda) > 0$, which corresponds to the number (counting multiplicity) of unstable eigenvalues of the NLEP (5.12).

To determine N, we calculate the winding of $\zeta(\lambda)$ over the Nyquist contour Γ traversed in the counterclockwise direction that consists of the positive and negative imaginary axis, defined by Γ_I^+ ($0 < \text{Im}(\lambda) < iR$, $\text{Re}(\lambda) = 0$) and Γ_I^- ($-iR < \text{Im}(\lambda) < 0$, $\text{Re}(\lambda) = 0$) respectively, together with the semi-circle C_R defined by $|\lambda| = R > 0$ for $|\arg(\lambda)| < \pi/2$. From (5.13b), $\mathcal{C}_c(\lambda)$ is a meromorphic function with a simple pole at $\lambda = 3$, whereas $\mathcal{F}(\lambda)$ is analytic in $\text{Re}(\lambda) \geq 0$ except at the simple pole at $\lambda = 3$. The simple poles of $\mathcal{C}(\lambda)$ and $\mathcal{F}(\lambda)$ do not cancel as $\lambda \to 3^-$, since when restricted to the real line we have $\mathcal{F}(\lambda) \to +\infty$ while $\mathcal{C}(\lambda) \to -\infty$ as $\lambda \to 3^-$. Therefore, $\zeta(\lambda) = \mathcal{C}(\lambda) - \mathcal{F}(\lambda)$ has a simple pole at $\lambda = 3$. Then, since $\zeta(\lambda)$ is bounded on C_R as $R \to \infty$, and $\zeta(\overline{\lambda}) = \overline{\zeta(\lambda)}$, we let $R \to \infty$ and obtain from the argument principle that

$$N = 1 + \frac{1}{\pi}\left[\arg\zeta\right]_{\Gamma_I^+}.\tag{5.14}$$

Here $\left[\arg\zeta\right]_{\Gamma_I^+}$ denotes the change in the argument of ζ as $\lambda = i\lambda_I$ is traversed down the positive imaginary axis $0 < \lambda_I < \infty$.

To calculate this argument change, we let $\lambda = i\lambda_I$ and decompose $\zeta(i\lambda_I) = \zeta_R(\lambda_I) + i\zeta(\lambda_I)$ and $\mathcal{F}(i\lambda_I) = \mathcal{F}_R(\lambda_I) + i\mathcal{F}_I(\lambda_I)$, to obtain from (5.13) that

$$\text{Im}\left[\zeta(i\lambda_I)\right] \equiv \zeta_I(\lambda_I) = -\frac{b\lambda_I}{9 + \lambda_I^2} - \mathcal{F}_I(\lambda_I),\tag{5.15a}$$

where $b \equiv 9\left[2\kappa_q(q+2)(\lambda-3)\right]^{-1}$ and $\mathcal{F}_I(\lambda_I) \equiv \text{Im}\left[\mathcal{F}(i\lambda_I)\right]$ is given by

$$\mathcal{F}_I(\lambda_I) = \frac{\lambda_I \int w^{q+1}\left[L_0^2 + \lambda_I^2\right]^{-1} w^3}{\int w^{q+2}}.\tag{5.15b}$$

Proposition 4.3 of [22] established that $\mathcal{F}_I(\lambda_I) > 0$ on $\lambda_I > 0$ when $q = 2$. Based on the numerical evidence shown in Fig. 5, for both integer and non-integer values of q, we make the following conjecture:

Conjecture 5.1 *Consider $\mathcal{F}_I(\lambda_I) \equiv Im\left[\mathcal{F}(i\lambda_I)\right]$ as defined by (5.15b). Then, $\mathcal{F}_I(\lambda_I) > 0$ on $\lambda_I > 0$ holds for all $q > 1$.*
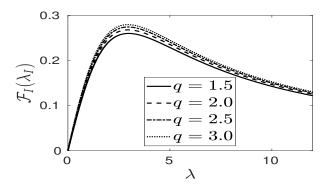
Figure 5: Plot of $\mathcal{F}_I(\lambda_I)$ versus λ_I, defined in (5.15b), for $q = 1.5, 2.0, 2.5, 3.0$ on the range $0 < \lambda_I < 12$. This function is rather insensitive to changes in q.

Assuming that this conjecture holds, we obtain the key inequality from (5.15a) that $\text{Im} \left[\zeta(i\lambda_I) \right] < 0$ for all $\lambda_I > 0$. Next, we observe that as $\lambda_I \to \infty$ we have $\zeta(i\lambda_I) \to \left(1 + \kappa_q + \mathcal{D}_u \right) / \left[\kappa_q(q+2) \right] > 0$, and that $\zeta(0) = \mathcal{C}_c(0) - 1/2$ satisfies

$$\zeta(0) > 0 \quad \text{if} \quad \mathcal{D}_u > \frac{1}{2} \left(1 + q\kappa_q \right) ; \qquad \zeta(0) < 0 \quad \text{if} \quad \mathcal{D}_u < \frac{1}{2} \left(1 + q\kappa_q \right) . \tag{5.16}$$

We readily conclude from these results that $[\arg \zeta]_{\Gamma_I^+} = 0$ when $\mathcal{D}_u > \frac{1}{2} \left(1 + q\kappa_q \right)$ and $[\arg \zeta]_{\Gamma_I^+} = -\pi$ when $\mathcal{D}_u < \frac{1}{2} \left(1 + q\kappa_q \right)$. From (5.14) it follows that $N = 1$ when $\mathcal{D}_u > \frac{1}{2} \left(1 + q\kappa_q \right)$ and that $N = 0$ otherwise. We summarize our result as follows:

Proposition 5.2 *Let $\tau = 0$ corresponding to an infinite police diffusivity, and assume that Conjecture 5.1 holds for $q > 1$. Then, under the conditions of Proposition 3.4, a multi-hotspot steady-state solution is unstable to asynchronous perturbations of the hotspot amplitudes for an arbitrary $q > 1$ when $\mathcal{D} > \mathcal{D}_c$, and is linearly stable to such perturbations whenever $\mathcal{D} < \mathcal{D}_c$. The instability when $\mathcal{D} > \mathcal{D}_c$ is due to a unique unstable eigenvalue in the spectrum of the NLEP (5.12). Here $\mathcal{D}_c$ is the competition threshold defined in (5.4).*

This result, valid only for an infinite police diffusivity, provides a necessary and sufficient condition for the linear stability of the multi-hotspot steady-state for an arbitrary $q > 1$. In the next section, we consider the effect of a finite police diffusivity, but only for the special case $q = 2$ corresponding to "cops-on-the-dots".

6 Asynchronous Perturbations: Linear Stability Analysis for $q = 2$

In this section we analyze the spectrum of the NLEP (3.20), relevant to asynchronous perturbations of the hotspot amplitudes, for the specific case of cops-on-the-dots where $q = 2$. For $q = 2$, in §6.1 we reformulate the NLEP (3.20) with three nonlocal terms into an NLEP with a single nonlocal term proportional to $\int w^3 \Phi$, which is then more readily analyzed. We will show that a finite police diffusivity leads to the possibility of oscillatory instabilities of the hotspot amplitudes when $\mathcal{D}$ is below the competition stability threshold.

6.1 Reformulation as an NLEP with One Nonlocal Term

For $q = 2$, the NLEP (3.20) for $\Phi \in L^2(\mathbb{R})$ has the form given in (4.23), where a, b, and c are now defined by

$$a \equiv \frac{4\chi_1}{\int w^4} , \qquad b \equiv \frac{3\chi_0}{\int w^3} , \qquad c \equiv \frac{2\chi_2}{\int w^2} , \tag{6.1}$$

in terms of χ_0, χ_1, and χ_2 as given in (3.20b).

We will convert the NLEP (4.23) with three nonlocal terms into an NLEP with a single nonlocal term proportional to $\int w^3\Phi$, instead of proportional to $\int w\Phi$ as in (4.29) of §4.2.1. This alternative reduction is needed for the study of asynchronous perturbations since from (3.20b) we have that χ_2, and thus c, vanishes linearly in λ as $\lambda \to 0$. With such a vanishing c, we would have that γ^{-1} in (4.29) is not analytic at $\lambda = 0$, which makes (4.29) problematic for analysis. As such, we require a different reformulation.

Let Φ and λ be any eigenpair of (4.23) with a, b, and c as defined in (6.1), in which $\lim_{\lambda \to 0} \lambda^{-1} c = c_0$ where c_0 is finite and non-zero. Then, proceeding as in the derivation of (4.25a) and (4.25b) we obtain the matrix system

$$\begin{pmatrix} b\int w^4 & c\int w^4 + \lambda \\ 3 - \lambda - b\int w^5 & -c\int w^5 \end{pmatrix} \begin{pmatrix} \int w^2\Phi \\ \int w\Phi \end{pmatrix} = \begin{pmatrix} 2 - a\int w^4 \\ a\int w^5 \end{pmatrix} \int w^3\Phi\,. \tag{6.2}$$

By inverting the matrix in (6.2), we calculate that

$$\int w^2\Phi = \frac{-(2c + a\lambda)\int w^5}{b\lambda\int w^5 - \left(c\int w^4 + \lambda\right)(3-\lambda)}\int w^3\Phi\,, \qquad \int w\Phi = \frac{(\lambda-3)(2 - a\int w^4) + 2b\int w^5}{b\lambda\int w^5 - \left(c\int w^4 + \lambda\right)(3-\lambda)}\int w^3\Phi\,, \tag{6.3}$$

provided that

$$b\lambda\int w^5 - \left(c\int w^4 + \lambda\right)(3-\lambda) \neq 0\,. \tag{6.4}$$

By substituting (6.3) into (4.23), we obtain after some algebra, the following NLEP with a single nonlocal term:

$$L_0\Phi - \chi w^3 \frac{\int w^3\Phi}{\int w^4} = \lambda\Phi\,, \qquad \text{where} \qquad \chi = \frac{(\lambda-3)(2c + a\lambda)\int w^4}{b\lambda\int w^5 - \left(c\int w^4 + \lambda\right)(3-\lambda)}\,. \tag{6.5}$$

Remark 6.1 *The multiplier χ in the NLEP (6.5) is well-defined at $\lambda = 0$ when $\lim_{\lambda \to 0} c/\lambda = c_0$ with c_0 finite and non-zero. This case is relevant to the study of the linear stability of asynchronous perturbations of the hotspot amplitudes.*

We have so far established that, provided the condition (6.4) holds, an eigenpair of (4.23) is also an eigenpair of (6.5). To complete the equivalence between (4.23) and (6.5), we now suppose that Φ, λ is an eigenpair of (6.5). Upon multiplying (6.5) by w^3, and then by w^2, we use the identities (4.24) to readily derive that

$$(2-\chi)\int w^3\Phi = \lambda\int w\Phi\,, \qquad (3-\lambda)\int w^2\Phi = \chi\frac{\int w^5}{\int w^4}\int w^3\Phi\,. \tag{6.6}$$

We then add and subtract in (6.5) to get

$$L_0\Phi - w^3\left[a\int w^3\Phi + b\int w^2\Phi + c\int w\Phi + \xi\right] = \lambda\Phi\,, \qquad \xi \equiv \left(\frac{\chi}{\int w^4} - a\right)\int w^3\Phi - b\int w^2\Phi - c\int w\Phi\,, \tag{6.7}$$

which reduces to (4.23) only when $\xi = 0$. We calculate using (6.6) that for $\lambda \neq 3$, and $\lim_{\lambda \to 0} c/\lambda$ finite and non-zero, that

$$\xi = \left(\frac{\chi}{\int w^4} - a - \frac{b\chi}{3-\lambda}\frac{\int w^5}{\int w^4} - \frac{c(2-\chi)}{\lambda}\right)\int w^3\Phi\,. \tag{6.8}$$

Finally, by using (6.5) for χ in (6.8), we get $\xi = 0$, so that (6.7) reduces to (4.23).

The relationship between the spectra of (4.23) and of (6.5) is summarized as follows:

Lemma 6.2 *Let Φ, λ, be an eigenpair of (4.23) where we assume that $\lim_{\lambda \to 0} c/\lambda$ is finite and non-zero. Moreover, suppose that (6.4) holds. Then, Φ, λ is an eigenpair of (6.5). Alternatively, if Φ, λ is an eigenpair of (6.5) with $\lambda \neq 3$, then if $\lim_{\lambda \to 0} c/\lambda$ is finite and non-zero, this eigenpair is also an eigenpair of (4.23).*

Next, by using (6.1) for c, and noting from the expression for χ_2 in (3.20b) that $\chi_2 = 0$ when $\lambda = 0$, we can eliminate the removable singularity at $\lambda = 0$ for χ, defined in (6.5), by rewriting

$$\chi = \frac{(\lambda - 3)(2c_0 + a)\int w^4}{b\int w^5 - (c_0\int w^4 + 1)(3 - \lambda)}, \qquad \text{where} \qquad c_0 \equiv \frac{c}{\lambda} = \frac{2\hat{\chi}_2}{\int w^2}, \qquad \hat{\chi}_2 \equiv \frac{\chi_2}{\lambda} = -\frac{\chi_0\tau_u\kappa_2}{\tau_u\lambda + 1}. \tag{6.9}$$

From (6.1), and by setting $q = 2$ in (3.20b), we obtain that the terms a and b in (6.9) are given explicitly by

$$a \equiv \frac{4\chi_0\kappa_2}{\int w^4}, \quad b \equiv \frac{3\chi_0}{\int w^3}, \qquad \text{where} \qquad \chi_0 \equiv \frac{1}{1 + \kappa_2 + \mathcal{D}_u}, \quad \kappa_2 = \frac{4U_0}{3\omega}, \quad \omega \equiv S(\gamma - \alpha) - \frac{4U_0}{3}. \tag{6.10}$$

In the usual way, it can be shown that the discrete spectra of the NLEP (6.5) are the roots of $\zeta(\lambda) = 0$ defined by

$$\zeta(\lambda) \equiv \mathcal{C}(\lambda) - \mathcal{F}(\lambda), \tag{6.11a}$$

where

$$\mathcal{C}(\lambda) \equiv \frac{1}{\chi(\lambda)} = \frac{b\int w^5 - (c_0\int w^4 + 1)(3 - \lambda)}{(\lambda - 3)(2c_0 + a)\int w^4}, \qquad \text{and} \qquad \mathcal{F}(\lambda) \equiv \frac{\int w^3(L_0 - \lambda)^{-1}w^3}{\int w^4}. \tag{6.11b}$$

By substituting (6.10) into (6.11b), we obtain after some rather lengthy, but straightforward, algebra that

$$\mathcal{C}(\lambda) = \frac{1}{2} + \frac{1}{4\kappa_2}\left(\frac{\tau_u\lambda + 1}{\tau_u\lambda + 1 - \frac{4\tau_u}{3}}\right)\left(1 + \mathcal{D}_u - \kappa_2 + \frac{9}{2(\lambda - 3)}\right). \tag{6.11c}$$

In addition, by using $L_0 w = 2w^3$, we can more conveniently rewrite $\mathcal{F}(\lambda)$ in (6.11b) as

$$\mathcal{F}(\lambda) = \frac{1}{2\int w^4}\int w^3(L_0 - \lambda)^{-1}\left[(L_0 - \lambda) + \lambda\right]w = \frac{1}{2} + \frac{\lambda}{2\int w^4}\int w^3(L_0 - \lambda)^{-1}w. \tag{6.11d}$$

As a remark, we can use (6.11) to recover the competition stability threshold given in (5.2) when $q = 2$. To see this, we set $\lambda = 0$ in (6.11d) and (6.11c) to get $\mathcal{F}(0) = 1/2$ and

$$\mathcal{C}(0) = \frac{1}{2} + \frac{3}{4\kappa_2(3 - 4\tau_u)}\left[\mathcal{D}_u - \left(\kappa_2 + \frac{1}{2}\right)\right]. \tag{6.12}$$

Therefore, $\mathcal{C}(0) = 1/2$, so that $\zeta(0) = 0$ in (6.11a), when $\mathcal{D}_u = 1/2 + \kappa_2$. This zero-eigenvalue condition agrees with (5.2).

6.2 Parametrization of the Hopf Bifurcation Threshold

In this subsection, we use (6.11) to determine an explicit parameterization of any Hopf bifurcation for the NLEP (6.5). We set $\lambda = i\omega$, with $\omega > 0$, and obtain by setting $\zeta(i\omega) = 0$ in (6.11) that

$$\left(\frac{1 + i\omega\tau_u}{1 - \frac{4\tau_u}{3} + i\omega\tau_u}\right)\left(\frac{2}{9}(1 + \mathcal{D}_u - \kappa_2) + \frac{1}{i\omega - 3}\right) = \frac{8\kappa_2}{9}\left[\mathcal{F}(i\omega) - \frac{1}{2}\right]. \tag{6.13}$$

We then decompose $\mathcal{F}(i\omega)$ into real and imaginary parts to obtain from (6.11b) that

$$\mathcal{F}(i\omega) = \mathcal{F}_R(\omega) + i\mathcal{F}_I(\omega), \qquad \mathcal{F}_R(\omega) \equiv \frac{\int w^3 L_0\left[L_0^2 + \omega^2\right]^{-1}w^3}{\int w^4}, \qquad \mathcal{F}_I(\omega) \equiv \omega\frac{\int w^3(L_0^2 + \omega^2)^{-1}w^3}{\int w^4}. \tag{6.14}$$

To determine a parameterization of the Hopf bifurcation curve, we first multiply both sides of (6.13) by $i\omega\tau_u + 1 - 4\tau_u/3$, and then separate the resulting expression into real and imaginary parts. This yields that

$$\frac{2}{9}(1 + \mathcal{D}_u - \kappa_2) - \frac{3}{9 + \omega^2} + \frac{\tau_u\omega^2}{9 + \omega^2} = \frac{8\kappa_2}{9}\left(\mathcal{F}_R(\omega) - \frac{1}{2}\right)\left(1 - \frac{4\tau_u}{3}\right) - \frac{8\kappa_2\tau_u}{9}\omega\mathcal{F}_I(\omega), \tag{6.15a}$$

$$\frac{2\tau_u\omega}{9}(1 + \mathcal{D}_u - \kappa_2) - \frac{3\tau_u\omega}{9 + \omega^2} - \frac{\omega}{9 + \omega^2} = \frac{8\kappa_2}{9}\left(\tau_u\omega\left[\mathcal{F}_R(\omega) - \frac{1}{2}\right] + \left(1 - \frac{4\tau_u}{3}\right)\mathcal{F}_I(\omega)\right). \tag{6.15b}$$

We then solve (6.15a) for $\mathcal{D}_u$ and substitute the resulting expression into (6.15b). This yields a quadratic equation for τ_u.

In this way, we obtain the following parameterization, with parameter ω, for any Hopf bifurcation curve $\tau_u = \tau_u(\omega)$ and $\mathcal{D}_u = \mathcal{D}_u(\omega)$ for the NLEP (6.5):

$$\mathcal{D}_u = \kappa_2 - 1 + \frac{9}{2}\left(\frac{3}{9+\omega^2} + \frac{8\kappa_2}{9}\left[\mathcal{F}_R(\omega) - \frac{1}{2}\right] - \eta_0 \tau_u\right), \tag{6.16a}$$

where τ_u is a root of the quadratic equation

$$\eta_0 \tau_u^2 - \eta_1 \tau_u + \eta_2 = 0. \tag{6.16b}$$

Here η_0, η_1, and η_2 are defined by

$$\eta_0 \equiv \frac{\omega^2}{9+\omega^2} + \frac{32\kappa_2}{27}\left[\mathcal{F}_R(\omega) - \frac{1}{2}\right] + \frac{8\kappa_2\omega}{9}\mathcal{F}_I(\omega), \qquad \eta_1 \equiv \frac{32\kappa_2}{27\omega}\mathcal{F}_I(\omega), \qquad \eta_2 \equiv \frac{1}{9+\omega^2} + \frac{8\kappa_2}{9\omega}\mathcal{F}_I(\omega). \tag{6.16c}$$

Since $\mathcal{F}_I(\omega) > 0$ for $\omega > 0$ (see part (v) of Proposition 4.3 in [22]), it follows that $\eta_1 > 0$ and $\eta_2 > 0$ for $\omega > 0$. However, the sign of η_0 is unclear, owing to the fact that $\mathcal{F}_R(\omega) < 1/2$ for $\omega > 0$ (see the left panel of Fig. 4 of [22]).
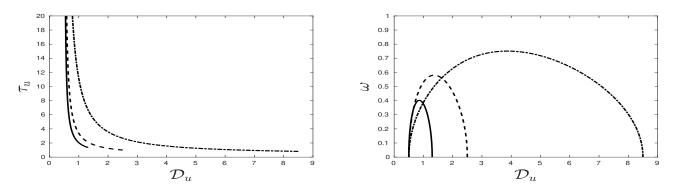

Figure 6: Left panel: the Hopf bifurcation threshold for "cops-on-the-dots" in the τ_u versus $\mathcal{D}_u$ plane, as computed from the parameterization (6.16), for $U_0 = 2$ (solid curve), $U_0 = 3$ (dashed curve), and $U_0 = 4$ (dot-dashed curve) when $S = 6$, $\gamma = 2$, and $\alpha = 1$. Right panel: the corresponding Hopf bifurcation frequency ω versus $\mathcal{D}_u$.

To calculate the Hopf bifurcation curve we fix $\kappa_2 > 0$ and let $\omega > 0$ be a parameter, and then numerically compute $\mathcal{F}_R(\omega)$ and $\mathcal{F}_I(\omega)$, as defined in (6.14), using a BVP solver. We then use (6.16b) to compute a $\tau_u > 0$, which determines $\mathcal{D}_u$ from (6.16a). In this way, in the left panel of Fig. 6 we plot the Hopf bifurcation threshold τ_u versus $\mathcal{D}_u$ for $U_0 = 2$, $U_0 = 3$, and $U_0 = 4$ for the fixed parameter set $S = 6$, $\gamma = 2$, and $\alpha = 1$. In addition, the Hopf frequency ω is plotted versus $\mathcal{D}_u$ in the right panel of Fig. 6. We emphasize that the Hopf curves in Fig. 6 are universal in the sense that, together with the relation (3.21) and (3.22), they provide Hopf bifurcation thresholds for each of the asynchronous modes $j = 1, \ldots, K-1$ in the $\mathcal{D}_p$ versus $\mathcal{D}$ parameter plane. In terms of these original parameters the Hopf curves are plotted in §7, where we will also provide a detailed comparison of the linear stability results with full PDE numerical simulations of (1.4).

An interesting feature, as observed in Fig. 6, is that the Hopf bifurcation frequency ω tends to zero at each of the two endpoints of the Hopf bifurcation curves, and that τ_u diverges at the lower endpoint in $\mathcal{D}_u$. To derive scaling laws for the Hopf thresholds at these two endpoints, we will take the limit $\omega \to 0$ in (6.16). To do so, we need the following lemma, as proved in Appendix B, which provides two-term expansions for $\mathcal{F}_R(\omega)$ and $\mathcal{F}_I(\omega)$ as $\omega \to 0$:

Lemma 6.3 As $\omega \to 0$, and with $w(y) = \sqrt{2}\operatorname{sech} y$, the real and imaginary parts of $\mathcal{F}(i\omega)$, as defined in (6.14), have the asymptotics

$$\mathcal{F}_R(\omega) \sim \frac{1}{2} - \frac{3}{64}\omega^2 + \mathcal{O}(\omega^2); \qquad \mathcal{F}_I(\omega) \sim \frac{3\omega}{16} + d_I\omega^3, \qquad d_I \equiv -\frac{\int y^2(w')^2}{16\int w^4} \approx -0.0285. \tag{6.17}$$

23

We substitute (6.17) into (6.16c) to obtain expressions for η_0, η_1, and η_2 for $\omega \to 0$. In this way, for $\omega \to 0$, (6.16b) becomes a singularly perturbed quadratic equation for τ_u

$$\omega^2 \tau_u^2 \left[1 + \kappa_2 + \mathcal{O}(\omega^2)\right] - 2\kappa_2 \tau_u \left(1 + \frac{16}{3}d_I\omega^2 + \mathcal{O}(\omega^4)\right) + 1 + \frac{3\kappa_2}{2} + \omega^2 \left(8\kappa_2 d_I - \frac{1}{9}\right) + \mathcal{O}(\omega^4) = 0. \tag{6.18}$$

For $\omega \to 0$, (6.18) has a small root with $\tau_u = \mathcal{O}(1)$ and a large root with $\tau_u = \mathcal{O}(\omega^{-2})$. By asymptotically calculating these two roots, and then using (6.16a) and (6.17) to determine $\mathcal{D}_u$, we readily obtain two scaling laws valid near each of the endpoints of the Hopf threshold curve shown in the left panel of Fig. 6.

In this way, we find that the small root corresponds to the right-hand endpoint of the Hopf curve, and for $\omega \to 0$

$$\tau_u \sim \tau_0 + \omega^2 \tau_1 + \cdots, \quad \mathcal{D}_u \sim \kappa_2 + \frac{1}{2} - \frac{\omega^2}{4}\left(\frac{19}{6} + \frac{9\kappa_2}{4} + \frac{1}{\kappa_2}\right); \quad \mathcal{D}_u \sim \kappa_2 + \frac{1}{2} - \frac{(\tau - \tau_0)}{4\tau_1}\left(\frac{19}{6} + \frac{9\kappa_2}{4} + \frac{1}{\kappa_2}\right), \tag{6.19a}$$

where τ_0 and τ_1 are defined by

$$\tau_0 \equiv \frac{3}{4} + \frac{1}{2\kappa_2}, \qquad \tau_1 \equiv \frac{(1 + \kappa_2)\left(1 + 3\kappa_2/2\right)^2}{8\kappa_2^3} - \frac{1}{18\kappa_2} - \frac{8d_I}{3\kappa_2}. \tag{6.19b}$$

In contrast, the large root of (6.18) corresponds to the left-hand endpoint of the Hopf curve. For $\omega \to 0$ we obtain

$$\tau_u \sim \left(\frac{2\kappa_2}{1 + \kappa_2}\right)\omega^{-2} + \mathcal{O}(1), \qquad \mathcal{D}_u \sim \frac{1}{2} + \omega^2 b, \qquad \text{where} \qquad b \equiv \frac{11}{24} + \kappa_2\left(\frac{3}{16} - \frac{16}{3}d_I\right) + \frac{1}{4\kappa_2}. \tag{6.20}$$

This yields the key scaling law for the left endpoint of the Hopf curve that

$$\tau_u \sim \left(\frac{2\kappa_2}{1 + \kappa_2}\right)\frac{b}{\mathcal{D}_u - 1/2}, \qquad \text{as} \qquad \mathcal{D}_u \to (1/2)^+. \tag{6.21}$$
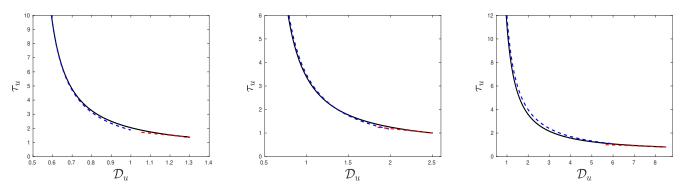

Figure 7: The Hopf bifurcation threshold for $U_0 = 2$ (left panel), $U_0 = 3$ (middle panel), and $U_0 = 4$ (right panel), when $S = 6$, $\gamma = 2$, and $\alpha = 1$, computed numerically from the parameterization (6.16) (solid curves). The dashed curves are the asymptotics for small ω near the right endpoint (6.19) (red curves) and the left endpoint (6.21) (blue curves). The asymptotic approximations are seen to provide a good approximation to almost the entire Hopf bifurcation curve.

In Fig. 7 we compare the two asymptotic approximations (6.19) and (6.21) with results computed numerically from the parameterization (6.16) for the same parameter values as in Fig. 6. Rather remarkably, we observe that the asymptotic results provide a decent quantitative prediction of the *entire* Hopf bifurcation curve. This close agreement is due to the Hopf frequency ω being relatively small on the entire range of the Hopf curve (see the right panel of Fig. 6).

In Proposition 6.4 given below in §6.3 we prove that a multi-hotspot steady-state is unstable whenever $\mathcal{D} > \mathcal{D}_c \equiv \kappa_2 + 1/2$ *for any $\tau_u > 0$*. This result is complementary to that in §5.1 where we proved a similar instability result for any $q > 1$,

but with $\tau_u = 0$. For the range $\mathcal{D} < \mathcal{D}_c$, we conjecture that the Hopf bifurcation curve in Fig. 7 sets the linear stability boundary in the τ_u versus $\mathcal{D}_u$ parameter space. This assertion is based on a continuation argument in τ_u. Recall from Proposition 5.2 that for $\tau_u = 0$, the NLEP (3.20) has no unstable eigenvalues when $\mathcal{D} < \mathcal{D}_c$. By increasing τ_u for fixed $\mathcal{D}_u < \mathcal{D}_c$, our parameterization (6.16) has shown that eigenvalues of (6.5) can occur on the imaginary axis $\lambda = i\omega$, with $\omega > 0$, only on the range $1/2 < \mathcal{D}_u < \mathcal{D}_c$. For $0 < \mathcal{D}_u < 1/2$, there are no purely imaginary eigenvalues for (6.5) for any $\tau_u > 0$, suggesting by continuity that $\mathrm{Re}(\lambda) \leq 0$ for (6.5). This suggests that below the Hopf bifurcation curve, the multi-hotspot pattern is linearly stable, and that this hotspot steady-state is linearly stable for all $\tau_u > 0$ when $\mathcal{D}_u < 1/2$. A computational tool to investigate this conjecture is formulated in §6.3.

6.3 An Instability Result and the Winding Number Criterion

For the analysis below, for $\tau_u > 0$ it is convenient to express $\mathcal{C}(\lambda)$ in (6.11c) in terms of partial fractions as

$$\mathcal{C}(\lambda) = c_0 + \frac{c_1}{\lambda - 3} + \frac{c_2}{\lambda - \lambda_p}, \qquad \lambda_p \equiv \frac{4}{3} - \frac{1}{\tau_u}, \tag{6.22a}$$

where $\lambda_p > 0$ iff $0 < \tau_u < 3/4$. In (6.22a), the coefficients c_0, $c_1 > 0$, and c_2 are

$$c_0 = \frac{1}{4}\left[1 + \frac{1}{\kappa_2}(1 + \mathcal{D}_u)\right], \quad c_1 = \frac{9}{8\kappa_2}\left(\frac{9\tau_u + 3}{5\tau_u + 3}\right), \quad c_2 = \frac{1}{\kappa_2}\left(\frac{1}{5\tau_u + 3}\right)\left[(1 + \mathcal{D}_u - \kappa_2)\left(\frac{5\tau_u}{3} + 1\right) - \frac{9\tau_u}{2}\right]. \tag{6.22b}$$

Our instability result is as follows:

Proposition 6.4 *For any $\tau_u > 0$, and for $q = 2$, a multi-hotspot steady-state solution is unstable to asynchronous perturbations of the hotspot amplitudes when $\mathcal{D} > \mathcal{D}_c \equiv \kappa_2 + 1/2$.*

Proof: We need to prove that $\zeta(\lambda)$, defined in (6.11a), has a real positive root whenever $\tau_u > 0$ and $\mathcal{D} > \mathcal{D}_c$. To do so, we consider three ranges of τ_u. When $\tau_u < 3/4$, we have from (6.22a) that $\mathcal{C}(\lambda)$ is continuous on $0 < \lambda < 3$, with $\mathcal{C}(\lambda) \to -\infty$ as $\lambda \to 3^-$. In addition, from (6.12), we have $\mathcal{C}(0) > 1/2$ when $\mathcal{D} > \mathcal{D}_c$. From (6.11b) we have $\mathcal{F}(0) = 1/2$, $\mathcal{F}(\lambda)$ continuous on $0 < \lambda < 3$, and $\mathcal{F}(\lambda) \to +\infty$ as $\lambda \to 3^-$ (cf. [22]). Therefore, by the intermediate value theorem, there is a real root to $\zeta(\lambda) = 0$ on $0 < \lambda < 3$. When $\tau_u > 3/4$, (6.12) yields that $\mathcal{C}(0) < 1/2$ when $\mathcal{D}_u > \mathcal{D}_c$, while (6.22a) shows that $\mathcal{C}(\lambda)$ has a simple pole at $\lambda = \lambda_p \equiv 4/3 - 1/\tau_u$ in $0 < \lambda_p < 3$. Regardless of the sign of c_2 in (6.22b), it readily follows that $\zeta(\lambda) = 0$ has a real positive root in $0 < \lambda < 3$. Finally, suppose that $\tau_u = 3/4$. Then, from (6.22) we have that $\mathcal{C}(\lambda) \to c_2/\lambda$ as $\lambda \to 0$, with $c_2 = [\mathcal{D}_u - (\kappa_2 + 1/2)]/(3\kappa_2) > 0$ when $\mathcal{D}_u > \kappa_2 + 1/2$. Therefore, since $\mathcal{C}(\lambda) \to -\infty$ as $\lambda \to 3^-$, while $\mathcal{C}(\lambda) \to +\infty$ as $\lambda \to 0^+$ when $\mathcal{D}_u > \kappa_2 + 1/2$, it follows that $\zeta(\lambda) = 0$ has a root on $0 < \lambda < 3$. $\blacksquare$

Next, we derive a winding number criterion that can be implemented numerically to count the number N of unstable eigenvalues of the NLEP (6.5). This hybrid analytical-numerical approach will be useful for considering the range $\mathcal{D} < \mathcal{D}_c$ and $\tau_u \neq 3/4$. For $\tau_u \neq 3/4$, $\mathcal{C}(\lambda)$ in (6.22) is analytic in $\mathrm{Re}(\lambda) \geq 0$ except for a simple pole at $\lambda = 3$, and an additional simple pole at $\lambda = \lambda_p > 0$ iff $\tau_u > 3/4$. From a winding number analysis, analogous to that developed in §5.1, the number N of roots of $\zeta(\lambda) = 0$ in $\mathrm{Re}(\lambda) > 0$, which is equivalent to the number of unstable eigenvalues of the NLEP (6.5), is

$$N = P + \frac{1}{\pi}[\arg\zeta]_{\Gamma_I^+}, \qquad P = \begin{cases} 1, & 0 < \tau_u < 3/4 \\ 2, & \tau_u > 3/4 \end{cases}. \tag{6.23a}$$

Here Γ_{I^+} is the positive imaginary axis traversed in the downwards direction. To numerically calculate $[\arg\zeta]_{\Gamma_I^+}$, we let $\lambda = i\omega$ with $\omega > 0$, and decompose $\zeta(i\omega) = \zeta_R(\omega) + i\zeta_I(\omega)$. Since $\zeta(i\omega) = \mathcal{C}(i\omega) - \mathcal{F}(i\omega)$, we use (6.14) for $\mathcal{F}(i\omega)$ together

with (6.22) to calculate $\mathcal{C}(i\omega)$. This yields that

$$\zeta_R(\omega) = c_0 - \frac{3c_1}{9 + \omega^2} - \frac{\lambda_p c_2}{\lambda_p^2 + \omega^2} - \mathcal{F}_R(\omega), \qquad \zeta_I(\omega) = -\frac{\omega}{(9 + \omega^2)(\lambda_p^2 + \omega^2)} \left[(c_1 + c_2)\,\omega^2 + c_1\lambda_p^2 + 9c_2 \right] - \mathcal{F}_I(\omega). \quad (6.23b)$$

Here $\mathcal{F}_R(\omega)$ and $\mathcal{F}_I\omega)$ can be calculated numerically from (6.14), while c_0, c_1, and c_2 are evaluated using (6.22b).

Figure 8: Plots of the path $\zeta(i\omega) = \zeta_R(\omega) + i\zeta_I(\omega)$ for $\mathcal{D}_u = 0.4$ (left panel) and $\mathcal{D}_u = 1.0$ (right panel) on $0 < \omega < \infty$, when $S = 6$, $\gamma = 2$, and $\alpha = 1$, corresponding to the left panel of Fig. 7. Left panel: $\tau_u = 0.4$ (dashed curve), $\tau_u = 5.0$ (solid curve), for which $[\arg \zeta]_{\Gamma_I^+} = -\pi$ and $[\arg \zeta]_{\Gamma_I^+} = -2\pi$, respectively. For both values of τ_u, (6.23a) yields $N = 0$. Right panel: $\tau_u = 1.0$ (dashed curve), $\tau_u = 4.0$ (solid curve), for which $[\arg \zeta]_{\Gamma_I^+} = -2\pi$ and $[\arg \zeta]_{\Gamma_I^+} = 0$, respectively. Then, (6.23a) yields $N = 0$ for $\tau_u = 1.0$ and $N = 2$ for $\tau_u = 4.0$. These results are consistent with the linear stability phase diagram in the left panel of Fig. 7.

To illustrate the use of (6.23b), we consider the phase diagram in the τ_u versus $\mathcal{D}_u$ shown in Fig. 7 where $U_0 = 2$, $S = 6$, $\gamma = 2$, and $\alpha = 1$. There, we predicted that there are no unstable eigenvalues of the NLEP when $\mathcal{D}_u < 0.5$. For $0.5 < \mathcal{D}_u < \kappa_2 + 1/2 = 1.3$, we predicted that there are no unstable eigenvalues of the NLEP when τ_u is below the Hopf bifurcation threshold. For particular parameter values, in Fig. 8 we show that a numerical implementation of the winding number criterion (6.23) confirms these predictions. Further numerical results using (6.23) for other parameter sets, and in particular for the middle and right panels of Fig. 7, confirms the linear stability predictions of §6.2.

7   Comparison of Linear Stability Theory with PDE Simulations: $q = 2$

We first map the phase diagrams for linear stability from the τ_u versus $\mathcal{D}_u$ plane of §6 for $q = 2$ to that of the ϵD_p versus $\mathcal{D}$ parameter plane. By setting $q = 2$ in (3.21) and (3.22), we obtain in terms of τ_u and $\mathcal{D}_u$ that

$$\mathcal{D} = \frac{\omega^3 S \mathcal{D}_u}{4K^4 \alpha^2 \pi^2 \left[1 - \cos\left(\frac{\pi j}{K}\right) \right]}, \qquad \epsilon D_p = \frac{S\omega^2}{K^3 \alpha^2 \pi^2 \left[1 - \cos\left(\frac{\pi j}{K}\right) \right]} \left(\frac{1}{\tau_u} \right), \qquad \text{for} \quad j = 1, \dots, K - 1, \qquad (7.1)$$

where $\omega = S(\gamma - \alpha) - 4U_0/3$. From (5.4), the competition instability threshold when $q = 2$ with $K \geq 2$ hotspots is

$$\mathcal{D}_c = \frac{\omega^3 S}{4K^4 \alpha^2 \pi^2 \left[1 + \cos\left(\pi/K\right) \right]} \left(\kappa_2 + \frac{1}{2} \right), \qquad \text{where} \quad \kappa_2 = \frac{4U_0}{3\omega}. \qquad (7.2)$$
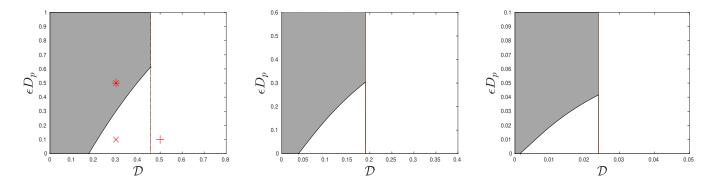
26

Figure 9: *The linear stability phase diagram for a two-hotspot steady-state in the ϵD_p versus $\mathcal{D}$ parameter plane for cops-on-the-dots, as obtained from (7.1), when $S = 6$, $\gamma = 2$, and $\alpha = 1$. Left panel: $U_0 = 2$. Middle Panel: $U_0 = 3$. Right Panel: $U_0 = 4$. The thin vertical line in each panel is the competition stability threshold $\mathcal{D}_c$ of (7.2), which decreases rather substantially as U_0 increases. The shaded region is where the steady-state two-hotspot pattern is linearly stable. For $\mathcal{D} > \mathcal{D}_c$ the hotspot solution is unstable due to a competition instability, whereas in the unshaded region for $\mathcal{D} < \mathcal{D}_c$, the hotspot steady-state is unstable to an asynchronous oscillatory instability of the hotspot amplitudes. PDE simulations of (1.4) at the marked points in the left panel are shown in Fig. 11.*
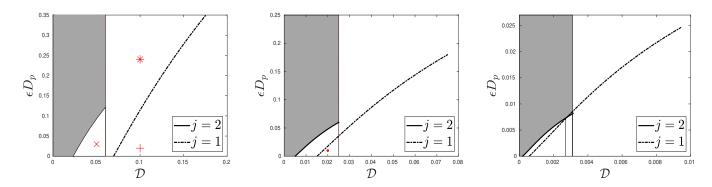

Figure 10: *The linear stability phase diagram for a three-hotspot steady-state in the ϵD_p versus $\mathcal{D}$ parameter plane for cops-on-the-dots, as obtained from (7.1), when $S = 6$, $\gamma = 2$, and $\alpha = 1$. Left panel: $U_0 = 2$. Middle Panel: $U_0 = 3$. Right Panel: $U_0 = 4$. The three-hotspot steady-state is linearly stable in the shaded region. The solid and dot-dashed curves are the Hopf bifurcation boundaries for the (sign-alternating) $j = 2$ mode and the $j = 1$ mode, respectively. This steady-state undergoes an oscillatory instability below the solid or dot-dashed curves. In each panel, the thin vertical line at the right edge of the shaded region is the competition stability threshold $\mathcal{D}_c$ of (7.2). The additional thin vertical line in the right panel for $U_0 = 4$ is where the Hopf boundary switches from the $j = 2$ to the $j = 1$ mode. PDE simulations of (1.4) at the marked points in the left panel and at the marked point in the middle panel are shown in Fig. 12 and Fig. 13, respectively.*

The mapping (7.1), combined with the Hopf parameterization in the τ_u versus $\mathcal{D}_u$ plane as given by (6.16), is readily implemented numerically to determine a linear stability phase diagram in the ϵD_p versus $\mathcal{D}$ parameter plane, representing the diffusivity of the police and criminals, respectively. For three different values of U_0, in Fig. 9 we plot this linear stability phase diagram for a two-hotspot steady-state for the parameter set $S = 6$, $\gamma = 2$, and $\alpha = 1$. A similar plot is shown in Fig. 10 for a three-hotspot steady-state.

For various points in the ϵD_p versus $\mathcal{D}_0$ parameter plane, we now validate our linear stability results by using the PDE software VLUGR [2] to compute full numerical simulations of the RD system (1.4) with 1000 meshpoints. For the initial

condition for (1.4) we use a perturbation of the K-hotspot steady-state solution (see Corollary 2.2), given by

$$A(x,0) = \frac{1}{\epsilon\sqrt{v_0}} \sum_{j=1}^{K} (1 + 0.01 a_j)\, w\left[\epsilon^{-1}(x - x_j)\right] + \alpha \left(1 - \sum_{j=1}^{K} e^{-(x-x_j)^2/\epsilon^2}\right), \tag{7.3a}$$

$$\rho(x,0) = \sum_{j=1}^{K} \left(w[\epsilon^{-1}(x - x_j)]\right)^2, \qquad U(x,0) = \frac{U_0}{4\epsilon K} \sum_{j=1}^{K} \left(w[\epsilon^{-1}(x - x_j)]\right)^2, \tag{7.3b}$$

where the hotspot locations are at their steady-state values $x_j = S(2j - 1)/(2K)$ for $j = 1, \ldots, K$. In (7.3a), the random coefficient a_j of the 1% perturbation of the hotspot amplitudes is taken to be uniformly distributed in $[-1, 1]$. For the PDE simulations reported below, we plot the amplitudes of the maxima of A versus t for the baseline parameter set $S = 6$, $\gamma = 2$, and $\alpha = 1$.
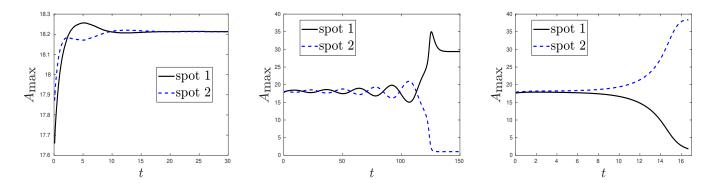

Figure 11: *The spot amplitudes computed numerically from the full PDE system (1.4) for a two-spot pattern with $S = 6$, $\gamma = 2$, $\alpha = 1$, $U_0 = 2$, $\epsilon = 0.03$, and $q = 2$ (cops-on-the-dots), at each of the three marked points in the linear stability phase diagram shown in the left panel of Fig. 9. Left panel: $\mathcal{D}_0 = 0.3$ and $\epsilon D_p = 0.5$, so that $D_p \approx 16.67$ (∗ point). The spot amplitudes are stable to asynchronous oscillations and to the competition instability. Middle panel: $\mathcal{D}_0 = 0.3$ and $\epsilon D_p = 0.1$, so that $D_p \approx 3.33$ (× point). Spot amplitudes are unstable to asynchronous oscillations, leading to the oscillatory collapse of a hotspot. Right panel: $\mathcal{D}_0 = 0.5$ and $\epsilon D_p = 0.1$, so that $D_p \approx 3.33$ (+ point). Spot amplitudes are unstable to a competition instability, leading to the monotonic collapse of a hotspot. These results are consistent with the linear stability predictions in the left panel of Fig. 9.*

For a two-hotspot solution, in Fig. 11 we validate our linear stability predictions shown in the left panel of Fig. 9 for $U_0 = 2$ and $\epsilon = 0.03$. The numerical results shown in Fig. 9 suggest that the asynchronous hotspot oscillations, due to a Hopf bifurcation, and the competition instability, due to a positive real eigenvalue, are both subcritical instabilities.
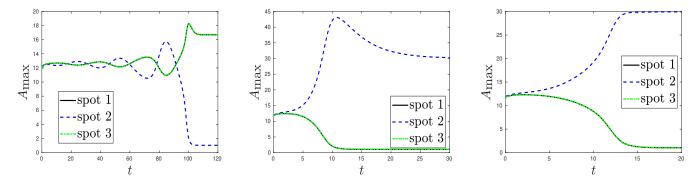
Figure 12: The spot amplitudes computed numerically from the full PDE system (1.4) for a three-spot pattern with $S = 6$, $\gamma = 2$, $\alpha = 1$, $U_0 = 2$, $\epsilon = 0.03$, and $q = 2$ (cops-on-the-dots), at each of the three marked points in the linear stability phase diagram shown in the left panel of Fig. 10. Left panel: $\mathcal{D}_0 = 0.05$ and $\epsilon D_p = 0.03$, so that $D_p = 1$ (× point). The spot amplitudes are unstable to asynchronous oscillations for the sign-altering $j = 1$ mode, which leads to the oscillatory collapse of the middle hotspot. The first and third hotspots are essentially synchronized. Middle panel: $\mathcal{D}_0 = 0.1$ and $\epsilon D_p = 0.02$, so that $D_p \approx 0.667$ (+ point). Spot amplitudes are unstable to asynchronous oscillations to the $j = 2$ mode, and are unstable to a competition instability for the sign-altering $j = 1$ mode. The latter instability has a larger growth-rate. An overshoot behavior, followed by a collapse of the (essentially synchronous) first and third hotspots is observed. Right panel: $\mathcal{D}_0 = 0.1$ and $\epsilon D_p = 0.24$, so that $D_p = 8$ (∗ point). Spot amplitudes are unstable to a competition instability for the sign-altering mode, but are now linearly stable to the $j = 2$ oscillatory mode. A monotonic collapse of the first and third hotspots is observed. These results are consistent with the linear stability predictions in the left panel of Fig. 10.

For a three-hotspot solution, PDE simulations of (1.4) are shown in Fig. 12 at each of the three marked points in the linear stability phase diagram given in the left panel of Fig. 10. As discussed in the figure caption of Fig. 12, these results again confirm the prediction of our linear stability analysis. For the parameter set corresponding to the middle panel of Fig. 12, the hotspot steady-state is unstable to both a competition instability, due to the sign-altering $j = 1$ mode, as well as an oscillatory instability for the $j = 2$ mode, which would lead to anti-phase oscillations between the first and third hotspots. However, since the linear growth-rate for such anti-phase oscillations is rather small (see the right panel of Fig. 6), the competition instability, which is due to a positive eigenvalue in the spectrum of the NLEP, is the dominant instability.

Finally, in Fig. 13 we plot the numerically computed hotspot amplitudes, obtained from a PDE simulation of (1.4), at the marked point in the middle panel of Fig. 10. For this parameter set, the three-hotspot steady-state is unstable to both sign-altering ($j = 1$) and anti-phase ($j = 2$) temporal oscillations. The numerical results in Fig. 13 show that the sign-altering mode is dominant and that small amplitude oscillations persist over rather long time intervals. In contrast to the likely subcritical behavior observed in the left panel of Fig. 12, for this parameter set the results in Fig. 13 suggest a supercritical oscillatory instability.

8   Discussion

We focus here on summarizing some of our main linear stability results for steady-state hotspot solutions of (1.4) for the special case $q = 2$ of "cops-on-the-dots"; a PDE model originally derived in [10] from the continuum limit of an agent-based model of urban crime with police intervention. For $q = 2$, our hybrid asymptotic-numerical analysis of the NLEP linear stability problem has provided phase diagrams in the ϵD_p versus $\mathcal{D}$ parameter space characterizing the linear stability properties of multi-hotspot steady-states for (1.4). For $\mathcal{D}$ exceeding the threshold $\mathcal{D}_c$ given by (7.2), referred to as the competition stability threshold, we proved in Proposition 6.4 that multi-hotspot steady-state solutions are unstable for all police diffusivities $D_p > 0$. On the intermediate range of $\mathcal{D}$ given by $\mathcal{D}^\star < \mathcal{D} < \mathcal{D}_c$, for some $\mathcal{D}^\star > 0$, our linear stability theory predicts that asynchronous hotspot amplitude oscillations will occur only if the police diffusivity is below some Hopf
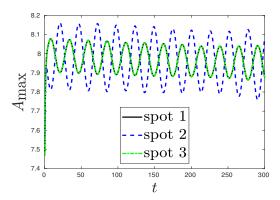
Figure 13: The spot amplitudes computed numerically from the full PDE system (1.4) for a three-spot pattern with $S = 6$, $\gamma = 2$, $\alpha = 1$, $U_0 = 3$, $\epsilon = 0.03$, and $q = 2$ (cops-on-the-dots), at the marked point in the middle panel of the phase diagram in Fig. 10 where $\mathcal{D}_0 = 0.02$ and $\epsilon D_p = 0.01$, so that $D_p \approx 0.333$. The spot amplitudes are unstable to both asynchronous oscillations for the sign-altering $j = 1$ mode and the anti-phase mode $j = 2$. Long-lived small-amplitude temporal oscillations that synchronize the first and third hotspots are observed.

bifurcation threshold. The interpretation of this oscillatory behavior is that a sufficiently "sluggish" police intervention has the effect of only displacing crime between adjacent hotspots. In §4, and more specifically in §4.2.1, we have established through a detailed analysis of the additional NLEP given in (3.18) that a one-hotpot steady-state is linearly stable, and that a multi-hotspot steady-state is always linearly stable to synchronous perturbations of the hotspot amplitudes. Finally, in §7 our linear stability predictions were validated from full PDE numerical simulations of (1.4).

For the case $q = 2$ of "cops-on-the-dots", we now compare the linear stability results obtained in [22] for the simple police interaction model, in which $-\rho U$ in (1.1b) is replaced by $-U$, with the results obtained herein for (1.4) for a predator-prey type police interaction. Although the overall qualitative shape of the various regions in the linear stability phase diagram of the ϵD_p versus $\mathcal{D}$ parameter plane is similar for the two models, there are two key quantitative differences. Firstly, the competition instability threshold value of $\mathcal{D}$ for (1.4) can be written as (see (7.2) with $q = 2$)

$$\mathcal{D}_c = \frac{S}{8K^4\pi^2\alpha^2\left[1 + \cos\left(\pi/K\right)\right]}g(\omega), \qquad \text{where} \quad g(\omega) \equiv -\omega^3 + 2S(\gamma - \alpha)\omega^2, \qquad \omega = S(\gamma - \alpha) - 4U_0/3, \qquad (8.1)$$

on $0 < U_0 < U_{0,\max} \equiv 3S(\gamma - \alpha)/4$. For the simple police interaction model studied in [22], (8.1) still holds but with ω replaced by $\omega_s \equiv S(\gamma - \alpha) - U_0$ (see equation (4.10) of [22]). For a given parameter set and fixed policing level U_0, since $\omega < \omega_s$ it follows that $\mathcal{D}_c$ is smaller for (1.4) than for the RD model in [22]. Consequently, the range of $\mathcal{D}$ where a K-hotspot pattern with $K \geq 2$ is unstable for all police diffusivities D_p is larger for (1.4) than it is for the RD model in [22]. Secondly, with regards to asynchronous hotspot oscillations for a two-hotspot solution, we observe by comparing the left panel of Fig. 9 with the left panel of Fig. 22 of [22] that the range of ϵD_p where these oscillations occur is smaller for (1.4) than it is for the RD model studied in [22], although the corresponding interval of $\mathcal{D}$ is roughly similar. A similar conclusion holds for a three-hotspot steady-state solution (compare left panels of Fig. 10 and Fig. 24 of [22]). This indicates that the parameter region where asynchronous hotspot oscillations occur is smaller for (1.4) than for the model studied in [22].

We now discuss a few open technical issues for our specific RD system (1.4). Firstly, in our NLEP linear stability analysis of (3.20) to characterize asynchronous hotspot amplitude oscillations, we focused primarily on the case $q = 2$ of "cops-on-the-dots", where the identities (4.24) were central for recasting the NLEP (3.20) with three nonlocal terms into the NLEP (6.5) with only one nonlocal term proportional to $\int w^3\Phi$. Since this special reduction is not available for $q \neq 2$, a

full numerical approach on the NLEP (3.20) would be needed to determine any Hopf bifurcation threshold for asynchronous oscillations when $q \neq 2$. Secondly, our construction of the steady-state for (1.4), and our derivation of the NLEP, required that $q > 1$. For $q = 1$, corresponding to a peripheral interdiction policing strategy (cf. [10]), the complicating feature of the analysis is that there is now a non-negligible police density both within the core of a hotspot and in the outer region away from the hotspots. This makes the asymptotic construction of a hotspot steady-state considerably more intricate, and leads to an NLEP with a rather different structure. Thirdly, for $q = 2$ it would be worthwhile to undertake a weakly nonlinear analysis to characterize the local branching behavior near a Hopf bifurcation point of the asynchronous hotspot amplitude oscillations. In contrast to the RD model of simple police interaction studied in [22], where only subcritical amplitude oscillations were found numerically, it appears that either subcritical or supercritical hotspot amplitude oscillations can occur for (1.4) (compare Fig. 11 and Fig. 12 with Fig. 13). The significance of analytically establishing the supercriticality of the Hopf bifurcation is that it would determine the parameter range where crime is only displaced temporally between neighboring hotspots over very long time intervals, without achieving a reduction in the overall total crime.

Finally, we briefly mention a few additional directions with a wider scope. For the RD system (1.4) it would be interesting to study hotspot patterns for the regime where $\mathcal{D} = \mathcal{O}(1)$. For the basic two-component crime model with no police intervention, it was shown in [21] that new hotspots of criminal activity can nucleate from an otherwise quiescent, largely crime-free, background, near a saddle-node bifurcation point of hotspot equilibria. It would be interesting to analyze whether this "peak-insertion" effect persists for (1.4) when the effect of police is included. Finally, it would be worthwhile to extend our 1-D analysis to a 2-D spatial domain to determine whether hotspot amplitudes in 2-D can undergo asynchronous temporal oscillations, leading to the temporal displacement of crime between neighboring spatial regions.

A   Derivation of the Jump Conditions: The NLEP

In this appendix we derive the BVPs (3.7) and (3.9), with jump conditions, that are needed to obtain the NLEP (3.20).

To derive the BVP (3.7) with a jump condition for ψ_x across the hotspot region, we integrate (3.2b) over an intermediate domain $-\delta < x < \delta$ with $\epsilon \ll \delta \ll 1$. We use the facts that $A_e \sim \epsilon^{-1} w / \sqrt{v_0}$, $\phi \sim \Phi(y)$, $A_e(\pm\delta) \sim \alpha$, and $u_e = \epsilon^{q-1} \tilde{u}_e$ as given in (2.14), to obtain, upon letting $\delta/\epsilon \to +\infty$, that

$$
\begin{aligned}
\epsilon \mathcal{D} \alpha^2 \left[\psi_x\right]_0 + 2\mathcal{D}_0 \alpha \left[v_{ex}\phi\right]_0 \;=\; & 3\epsilon \int_{-\infty}^{\infty} w^2 \Phi \, dy + \frac{\epsilon \psi(0)}{v_0^{3/2}} \int_{-\infty}^{\infty} w^3 \, dy \\
& + \frac{\epsilon(q+2)\tilde{u}_e}{v_0^{(q-1)/2}} \int_{-\infty}^{\infty} w^{q+1}\Phi \, dy + \frac{\epsilon \tilde{u}_e \psi(0)}{v_0^{1+q/2}} \int_{-\infty}^{\infty} w^{q+2} + \frac{\epsilon \eta(0)}{v_0^{q/2}} \int_{-\infty}^{\infty} w^{q+2} \, dy + \mathcal{O}(\epsilon^2 \lambda),
\end{aligned}
$$

where we have introduced the notation $[a]_0 \equiv a(0^+) - a(0^-)$ to indicate that the evaluation is to be done with the outer solution. In addition, we have used the shorthand notation that $\int (\ldots) \equiv \int_{-\infty}^{\infty} (\ldots) \, dy$. Since $\phi = \mathcal{O}(\epsilon^3)$ in the outer region from (3.6), we can neglect the second term on the left-hand side of the expression above. For eigenvalues for which $\lambda \ll \mathcal{O}(\epsilon^{-1})$, the expression above simplifies to

$$
\mathcal{D} \alpha^2 [\psi_x]_0 = 3 \int w^2 \Phi + \frac{\psi(0)}{v_0^{3/2}} \int w^3 + \frac{(q+2)\tilde{u}_e}{v_0^{(q-1)/2}} \int w^{q+1}\Phi + \frac{\tilde{u}_e \psi(0)}{v_0^{1+q/2}} \int w^{q+2} + \frac{\eta(0)}{v_0^{q/2}} \int w^q. \tag{A.1}
$$

Then, in (3.2b), we use $\phi = \mathcal{O}(\epsilon^3)$ in the outer region from (3.6), together with the fact $\epsilon^q \eta A_e^q \ll \mathcal{O}(\epsilon)$ since $q > 1$. In this way, (3.2b) and (A.1) yield the leading-order BVP problem for ψ given in (3.7) with a jump condition for ψ_x across $x = 0$:

To formulate a similar BVP for $\eta(x)$, we integrate (3.2c) over $-\delta < x < \delta$, with $\epsilon \ll \delta \ll 1$, and let $\delta/\epsilon \to \infty$ to obtain

$$
\mathcal{D} \epsilon^q \alpha^q \left[\eta_x\right]_0 + \mathcal{D} q \alpha^{q-1} \mathcal{O}(\epsilon^{q+2}) = \epsilon^3 \tau_u \lambda \left[\frac{q\tilde{u}_\epsilon}{v_0^{(q-1)/2}} \int w^{q-1}\Phi + \frac{\eta(0)}{v_0^{q/2}} \int w^q \right]. \tag{A.2}
$$

To obtain a distinguished balance in (A.2), we introduce $\hat{\tau}$ defined by $\hat{\tau} \equiv \epsilon^{3-q}\tau$ (see (3.8)). With this scaling, the police diffusivity $D_p \equiv \epsilon^{-2}\mathcal{D}/\tau$, is simply $D_p \equiv \epsilon^{1-q}\mathcal{D}/\hat{\tau}$. In this way, (A.2) yields the following jump condition for $\eta(x)$:

$$\mathcal{D}\alpha^q \left[\eta_x\right]_0 = \hat{\tau}\lambda \left[\frac{q\tilde{u}_e}{v_0^{(q-1)/2}} \int w^{q-1}\Phi + \frac{\eta(0)}{v_0^{q/2}} \int w^q\right]. \tag{A.3}$$

In the outer region we obtain from (3.2c) that

$$\mathcal{D}\epsilon^q\alpha^q\eta_{xx} + \mathcal{O}(\epsilon^{q+2}) = \epsilon^2\tau\lambda \left[\mathcal{O}(\epsilon^{q+2}) + \epsilon^q\alpha^q\eta\right]. \tag{A.4}$$

In our analysis, we consider the range of τ, and consequently $\hat{\tau}$, for which

$$\tau \ll \mathcal{O}(\epsilon^{-2}), \qquad \text{for which} \qquad \hat{\tau} \ll \mathcal{O}(\epsilon^{1-q}). \tag{A.5}$$

We will assume that $\hat{\tau} = \mathcal{O}(1)$, so that (A.5) or $\hat{\tau}$ holds for all $q > 1$. For this range, (A.4) reduces to $\eta_{xx} \approx 0$ to leading order. In this way, we obtain the BVP (3.9) for $\eta(x)$ with the specified jump condition for η_x across $x = 0$.

B   Proof of Lemma 6.3

We first determine $\mathcal{F}_R(\omega)$ in (6.14) for $\omega \to 0$. We use $(L_0^2 + \omega^2)^{-1} = L_0^{-2} - \omega^2 L_0^{-4} + \mathcal{O}(\omega^4)$ for $\omega \to 0$, to obtain that

$$\mathcal{F}_R(\omega) = \frac{\int w^3 L_0^{-1}w^3}{\int w^4} - \omega^2 \frac{\int w^3 L_0^{-3}w^3}{\int w^4} + \mathcal{O}(\omega^4). \tag{B.1}$$

Since $L_0^{-1}w = \frac{1}{2}(w + yw')$ and $L_0^{-1}w^3 = w/2$ (see equation (3.7) of [23]), we get using integration by parts that

$$\mathcal{F}_R(\omega) = \frac{1}{2} - \frac{\omega^2}{2\int w^4} \int w^3 L_0^{-2}w + \mathcal{O}(\omega^4) = \frac{1}{2} - \frac{\omega^2}{2\int w^4} \int \left(L_0^{-1}w^3\right)\left(L_0^{-1}w\right) + \mathcal{O}(\omega^4),$$

$$= \frac{1}{2} - \frac{\omega^2}{8\int w^4} \int w(w + yw') + \mathcal{O}(\omega^4) = \frac{1}{2} - \frac{\omega^2}{8\int w^4}\left[\int w^2 + \frac{1}{2}\int y(w^2)'\right]. \tag{B.2}$$

Upon integrating the last expression in (B.2) by parts, and then using $\int w^2/\int w^4 = 3/4$ from (2.5), we conclude that

$$\mathcal{F}_R(\omega) = \frac{1}{2} - \frac{\omega^2 \int w^2}{16\int w^4} + \mathcal{O}(\omega^4) = \frac{1}{2} - \frac{3\omega^2}{64} + \mathcal{O}(\omega^4), \qquad \text{as} \quad \omega \to 0. \tag{B.3}$$

This yields the result for $\mathcal{F}_R(\omega)$ given in (6.17) of Lemma 6.3.

Next, we derive the asymptotics of $\mathcal{F}_I(\omega)$ as $\omega \to 0$. By letting $\omega \to 0$ in (6.14) for $\mathcal{F}_I$, we obtain that

$$\mathcal{F}_I(\omega) = \omega\frac{\int w^3 L_0^{-2}w^3}{\int w^4} - \omega^3\frac{\int w^3 L_0^{-4}w^3}{\int w^4} + \mathcal{O}(\omega^5). \tag{B.4}$$

Upon integrating by parts, and then using $L_0^{-1}w^3 = w/2$ we obtain that

$$\mathcal{F}_I(\omega) = \omega\frac{\int \left(L_0^{-1}w^3\right)^2}{\int w^4} - \omega^3\frac{\int \left(L_0^{-1}w^3\right)\left(L_0^{-3}w^3\right)}{\int w^4} + \mathcal{O}(\omega^5) = \frac{\omega\int w^2}{4\int w^4} - \frac{\omega^3}{2\int w^4}\int wL_0^{-2}\left(L_0^{-1}w^3\right) + \mathcal{O}(\omega^5). \tag{B.5}$$

Next, we use $L_0^{-1}w^3 = w/2$, $\int w^2/\int w^4 = 3/4$, and $\int wL_0^{-2}w = \int \left(L_0^{-1}w\right)^2$ from integration by parts. Then, (B.5) becomes

$$\mathcal{F}_I(\omega) = \frac{3\omega}{16} - \frac{\omega^3}{4\int w^4}\int \left(L_0^{-1}w\right)^2 + \mathcal{O}(\omega^5). \tag{B.6}$$

Finally, we use $L_0^{-1}w = (w + yw')/2$, so that upon integration by parts (B.6) becomes

$$\mathcal{F}_I(\omega) = \frac{3\omega}{16} - \frac{\omega^3}{16\int w^4}\left[\int w^2 + \int y(w^2)' + \int y^2(w')^2\right] + \mathcal{O}(\omega^5) = \frac{3\omega}{16} - \frac{\omega^3}{16\int w^4}\int y^2(w')^2 + \mathcal{O}(\omega^5). \tag{B.7}$$

This completes the derivation of the two-term expansion of $\mathcal{F}_I(\omega)$ as $\omega \to 0$ given in (6.17) of Lemma 6.3. By using $\int w^4 = 16/3$ and $w = \sqrt{2}\,\mathrm{sech}(y)$, a numerical quadrature yields that $\mathcal{F}_I(\omega) = 3\omega/16 + d_I\omega^3 + \mathcal{O}(\omega^5)$, with $d_I \approx -0.0285$.

C   Proof of Lemma 4.1

In this appendix, we prove Lemma 4.1, i.e. we establish the following inequality

$$I_0[\Phi] = \int [(\Phi')^2 + \Phi^2 - 3w^2\Phi^2] + 3\frac{\int w^3\Phi \int w^2\Phi}{\int w^4} > 0, \quad \forall \Phi \not\equiv 0. \tag{C.1}$$

To this end, we consider the following quadratic form

$$Q_a[\Phi] \equiv \int [(\Phi')^2 + \Phi^2 - 3w^2\Phi^2] + 2a\frac{\int w^3\Phi \int w^2\Phi}{\int w^4} + 2b\frac{(\int w^3\Phi)^2}{\int w^4}, \tag{C.2}$$

where

$$b = \frac{5}{4} - a. \tag{C.3}$$

Note that $Q_0[\Phi] > 0$ by Lemma 5.1 of [27] (Here $p - 1 = 2$ in Lemma 5.1 of [27]). We observe that $Q_0[\Phi] = -\int \Phi\mathcal{L}\Phi$, where $\mathcal{L}$ is the self-adjoint linear operator

$$\mathcal{L}\Phi \equiv L_0\Phi - \left(a\frac{\int w^2\phi}{\int w^3} + 2b\frac{\int w^3\phi}{\int w^4}\right)w^3 - a\frac{\int w^3\phi}{\int w^3}w^2. \tag{C.4}$$

We will continue in the parameter a until we reach a point for which $\mathcal{L}$ has principal eigenvalue zero, i.e. there exists an eigenfunction satisfying $\mathcal{L}\Phi = 0$ for some $\Phi \not\equiv 0$. At this point, $Q_a[\Phi]$ ceases to be positive definite.

To study this zero-eigenvalue problem we set $c_1 = \int w^3\Phi$ and $c_2 = \int w^2\Phi$. We will use the identities $L_0^{-1}w^3 = \frac{1}{2}w$, $L_0^{-1}w^2 = \frac{1}{3}w^2$, $\int w^3 L_0^{-1}w^2 = \int w^2 L_0^{-1}w^3 = \frac{1}{2}\int w^3$, and $\int w^2 L_0^{-1}w^2 = \frac{1}{3}\int w^4$. Upon multiplying $\mathcal{L}\Phi = 0$ in (C.4) by w and integrating by parts, we get

$$c_1 = \left(a\frac{c_2}{\int w^3} + 2b\frac{c_1}{\int w^4}\right)\frac{\int w^4}{2} + \frac{a}{2}\frac{c_1}{\int w^3}\int w^3, \tag{C.5}$$

which yields

$$\left(b + \frac{a}{2} - 1\right)c_1 + \frac{a}{2}\frac{\int w^4}{\int w^3}c_2 = 0. \tag{C.6}$$

Similarly, we multiply $\mathcal{L}\Phi = 0$ by w^2 and integrate by parts to get

$$c_2 = \left(a\frac{c_2}{\int w^3} + 2b\frac{c_1}{\int w^4}\right)\frac{\int w^5}{3} + \frac{a}{3}\frac{c_1}{\int w^3}\int w^4. \tag{C.7}$$

Upon using $\int w^5 = (3/2)\int w^3$, (C.7) becomes

$$\left(\frac{a}{3}\frac{\int w^4}{\int w^3} + b\frac{\int w^3}{\int w^4}\right)c_1 + \left(\frac{a}{2} - 1\right)c_2 = 0. \tag{C.8}$$

The homogeneous linear system (C.6) and (C.8) for c_1 and c_2 has a nontrivial solution if and only if $H(a) = 0$, where

$$H(a) \equiv \left(b + \frac{a}{2} - 1\right)\left(\frac{a}{2} - 1\right) - \frac{a^2}{6}\left(\frac{\int w^4}{\int w^3}\right)^2 - \frac{ab}{2}. \tag{C.9}$$

Recalling the choice of b in (C.3), and using $\int w^4 = 16/3$ and $\int w^3 = \sqrt{2}\pi$, we readily calculate from (C.9) that

$$H(a) = -\frac{1}{4} + \left(\frac{1}{4} - \frac{64}{27\pi^2}\right)a^2. \tag{C.10}$$

We calculate that $H(0) < 0$ and $H(2) < 0$, so that $H(a) < 0$ for $a \in [0, 2]$.

In this way, we conclude that $Q_{\frac{3}{2}}[\Phi] > 0 \; \forall\Phi \not\equiv 0$, which means that

$$Q_{\frac{3}{2}}[\Phi] := \int \left[(\Phi')^2 + \Phi^2 - 3w^2\Phi^2\right] + 3\frac{\int w^3\Phi \int w^2\Phi}{\int w^4} - \frac{1}{2}\frac{(\int w^3\Phi)^2}{\int w^4} > 0, \tag{C.11}$$

and hence $I_0[\Phi] > 0$ as claimed. (If $\int w^3\Phi = 0$, then by Lemma 5.1 of [27], $I_0[\Phi] > 0$. If $\int w^3\Phi \neq 0$, then $I_0[\Phi] > 0$.)

Acknowledgments

References

[1] H. Berestycki, J. Wei, M. Winter, *Existence of symmetric and asymmetric spikes for a crime hotspot model*, SIAM J. Math. Anal., **46**(1), (2014), pp. 691–719.

[2] J. G. Blom, R. A. Trompert, J. G. Verwer, *Algorithm 758: VLUGR 2: A vectorizable adaptive grid solver for PDEs in 2D*, ACM Trans, Math. Softw., **22**(3), (1996), pp. 302–328.

[3] A. A. Braga, *The effects of hot spots policing on crime*, Ann. Am. Acad. Polit. S. S., **578**, (2001), pp. 104–125.

[4] P. L. Brantingham, P. J. Brantingham, *Crime patterns*, McMillan, (1987).

[5] A. Camacho, H. R. L. Lee, L. Smith, *Modeling policing strategies for departments with limited resources*, Europ. J. Appl. Math., **27**(3), (2016). pp. 479–501.

[6] R. Cantrell, C. Cosner, R. Manasevich, *Global bifurcation of solutions for crime modeling equations*, SIAM J. Math. Anal., **44**(3), (2012), pp. 1340–1358.

[7] A. Doelman, R. A. Gardner, T. J. Kaper, *Large stable pulse solutions in reaction-diffusion equations*, Indiana U. Math. J., **50**(1), (2001), pp. 443–507.

[8] Y. Gu, Q. Wang, G. Yi, *Stationary patterns and their selection mechanism of urban crime models with heterogeneous near-repeat victimization effect*, Europ. J. Appl. Math., **28**(1), (2017), pp. 141–178.

[9] S. Johnson, K. Bower, *Domestic burglary repeats and space-time clusters: The dimensions of risk*, Europ. J. of Criminology, **2**, (2005), pp. 67–92.

[10] P. A. Jones, P. J. Brantingham, L. Chayes, *Statistical models of criminal behavior: The effect of law enforcement actions*, Math. Models. Meth. Appl. Sci., **20**, Suppl., (2010), pp. 1397–1423.

[11] T. Kolokolnikov, M. J. Ward, J. Wei, *The stability of steady-state hot-spot patterns for a reaction-diffusion model of urban crime*, DCDS-B, **19**(5), (2014), p. 1373–1410.

[12] T. Kolokolnikov, M. J. Ward, J. Wei, *The existence and stability of spike equilibria in the one-dimensional Gray-Scott model: The low feed rate regime*, Studies in Appl. Math, **115**(1), (2005), pp. 21–71.

[13] D. J. B. Lloyd, H. O'Farrell, *On localised hotspots of an urban crime model*, Physica D, **253**, (2013), pp. 23–39.

[14] H. van der Ploeg, A. Doelman, *Stability of spatially periodic pulse patterns in a class of singularly perturbed reaction-diffusion equations*, Indiana Univ. Math. J., **54**(5), (2005), pp. 1219–1301

[15] A. B. Pitcher, *Adding police to a mathematical model of burglary*, Europ. J. Appl. Math., **21**(4-5), (2010), pp. 401–419.

[16] L. Ricketson, *A continuum model of residential burglary incorporating law enforcement*, unpublished, (2011). Retrieved from http://cims.nyu.edu/~lfr224/writeup.pdf.

[17] N. Rodriguez, A. Bertozzi, *Local existence and uniqueness of solutions to a PDE model for criminal behavior*, M3AS (special issue on Mathematics and Complexity in Human and Life Sciences), **20**(1), (2010), pp. 1425–1457.

[18] M. B. Short, M. R. D'Orsogna, V. B. Pasour, G. E. Tita, P. J. Brantingham, A. L. Bertozzi, L. B. Chayes, *A statistical model of criminal behavior*, Math. Models. Meth. Appl. Sci., **18**, Suppl., (2008), pp. 1249–1267.

[19] M. B. Short, A. L. Bertozzi, P. J. Brantingham *Nonlinear patterns in urban crime - hotspots, bifurcations, and suppression*, SIAM J. Appl. Dyn. Sys., **9**(2), (2010), pp. 462–483.

[20] M. B. Short, P. J. Brantingham, A. L. Bertozzi, G. E. Tita (2010), *Dissipation and displacement of hotspsots in reaction-diffusion models of crime*, Proc. Nat. Acad. Sci., **107**(9), pp. 3961-3965.

[21] W.-H. Tse, M. J. Ward, *Hotspot formation and dynamics for a continuum model of urban crime*, Europ. J. Appl. Math., **27**(3), (2016), pp. 583–624.

[22] W.-H. Tse, M. J. Ward, *Asynchronous instabilities of crime hotspots for a 1-D reaction-diffusion model of urban crime with focused police patrol*, SIAM J. Appl. Dyn. Sys., **17**(3), (2018), pp. 2018–2075.

[23] M. J. Ward, J. Wei, *Hopf bifurcations and oscillatory instabilities of spike solutions for the one-dimensional Gierer-Meinhardt model*, J. Nonlinear Sci., **13**(2), (2003), pp. 209–264.

[24] M. J. Ward, J. Wei, *Hopf bifurcation of spike solutions for the shadow Gierer-Meinhardt model*, Europ. J. Appl. Math., **14**(6), (2003), pp. 677–711.

[25] J. Wei, M. Winter, *A nonlocal eigenvalue problem and the stability of spikes for reaction-diffusion systems with fractional reaction rates*, Int. J. Bifur. Chaos **13**(6) (2003), pp. 1529–1543.

[26] J. Wei, M. Winter, *Spikes for the two-dimensional Gierer-Meinhardt system: the weak coupling case*, J. Nonlinear Sci., **11**(6), (2001), pp. 415–458.

[27] J. Wei, *On single interior spike solutions for the Gierer-Meinhardt system: uniqueness and stability estimates*, Europ. J. Appl. Math., **10**(4), (1999), pp. 353–378.

[28] J. Wei, *Existence and stability of spikes for the Gierer-Meinhardt system*, book chapter in *Handbook of Differential Equations, Stationary Partial Differential Equations*, Vol. 5 (M. Chipot ed.), Elsevier, (2008), pp. 489–581.

[29] J. Q. Wilson, G. L. Kelling, *Broken windows and police and neighborhood safety*, Atlantic Mon., **249**, (1998), pp. 29–38.

[30] J. R. Zipkin, M. B. Short, A. L. Bertozzi, *Cops on the dots in a mathematical model of urban crime and police response*, DCDS-B, **19**(5), (2014), pp. 1479–1506.